Low cost, multiscale and multi-sensor application for flooded areas mapping.

Daniele Giordan[1], Davide Notti[1], Alfredo Villa[2], Francesco Zucca[3], Fabiana Calò[4], Antonio Pepe[4], Furio Dutto[5], Paolo Pari[6], Marco Baldo[1], Paolo Allasia[1]

[1]National Research Council of Italy, Research Institute for Geo-Hydrological Protection (CNR-IRPI), Strada delle Cacce 73, Torino 10135. Italy;

[2]ALTEC S.p.A., Torino, 10146, Italy;

[3]Department of Earth and Environmental Science, University of Pavia, Via Ferrata 1, 27100 Pavia, Italy

[4]National Research Council of Italy, Institute for the Electromagnetic Sensing of the Environment (CNR-IREA), Via Diocleziano 328, Napoli 80124, Italy;

[5]Civil protection Service of Torino, Grugliasco, 10095, Italy;

[6]Digisky S.r.l., Torino, 10146, Italy.

Correspondence to: Davide Notti (davide.notti@irpi.cnr.it)

Abstract

Flood mapping and estimation of maximum water depth are essential elements for a first damages evaluation, civil protection interventions planning and detection of areas where remedial are more needed.

In this work, we present and discuss a methodology for mapping and quantifying flood severity over plain areas. The proposed methodology considers a multiscale and multi-sensor approach using free or low-cost data/sensors. We applied this method to November 2016 Piemonte (NW Italy) flood. We first mapped flooded areas at basin scale using free satellite data from low to medium-high resolution using both SAR (Sentinel-1, Cosmo-Skymed) and multispectral sensors (MODIS, Sentinel-2). Using very- and ultra- high-resolution images from the low-cost aerial platform and Remotely Piloted Aerial System, we refined the flooded zone, and we detected the most damaged sector. The presented method considers both urbanized and not urbanized areas. Nadiral images have several limitations in particular in urbanized areas, where the use of terrestrial images solved this limitation. Very- and ultra-high resolution images have been processed with Structure from Motion (SfM) for the realization of 3-D models. These data, combined with available digital elevation model, allowed us to obtain maps of flooded area, maximum water high and damaged infrastructures.

1 Introduction

Floods are among the natural disasters that cause significant damages and casualties (Barredo, 2007).

Mapping and modelling areas affected by floods is a crucial task to: i) identify the most critical areas for civil protection actions ii) evaluate damages, iii) and do correct urban planning. (Amadio et al., 2016). In order to make a precise quantification of damages, a detailed mapping of flooded areas is required, with a reasonable estimation of water level and flow velocity (Arrighi

et al., 2013; Luino et al., 2009; Merz et al., 2010; Kreibich, 2009). Advances in remote sensing and technology have introduced the possibility, in last years, of having rapid maps and models during or little time after a flood event (e.g., Copernicus Emergency Management Service (© European Union, 2012-2017)). With satellite remote sensing data, it is possible to map flood effects over vast areas at different spatial and temporal resolution using multispectral (Brakenridge, et al., 2006; Gianinetto et al.,2006; Nigro et al., 2014; Wang et al., 2012; Yan et al., 2015; Rahman and Di, 2017) or Synthetic Aperture Radar (SAR) images (Boni et al., 2016; Mason et al., 2014; Schumann et al., 2015; Refice et al., 2014; Pulvirenti et al., 2011; Clement et al., 2017; Brivio et al., 2002). A good description of main methodologies used to map flood with satellite data has been published by Fayne et al., (2017). Moreover, the increasing availability of free-of-charge satellite data with global coverage (e.g., Sentinel-1 and -2 from ESA, Landsat and MODIS satellites from NASA) makes possible analyses of flooded areas with low-cost solutions. Flood mapping and damages assessment is also an important issue for European Communities authorities that support projects like the Copernicus Emergency Management Service mapping (EMSR) and the European Flood Awareness System (EFAS), which manage the activation procedure to acquire satellite data over the areas affected by a natural hazard. De Moel et al., (2009) and Paprotny at al., (2017) described further details about different experiences in flood mapping in Europe.

In urban areas, remote sensing data are often less efficient in the detection of flooded areas, especially if images acquired during the maximum of inundation are not available. A partial solution could be the use of a Remotely Piloted Aerial Systems (RPAS) (Perks et al., 2016; Feng et al., 2015), that are usually able to acquire ultra-high resolution images over small areas. The quantification of the maximum water level caused by the inundation is a crucial parameter in particular in urban areas because it can supply the damages estimations and support civil protection operations (Luino et al., 2009; Bignami et al., 2017). Very often, nadiral remote sensed platforms cannot be able to the definition of the level of water and, for this reason, field surveys and ground-based photos are still necessary. A possible solution is the use of models for the estimation of water depth based on DTM or hydraulic model (Bates and De Roo, 2000; Segura-Beltrán et al., 2016), but ground truth validation is needed. Recent developments of computer vision applications like Structure from Motion (SfM) (Snavely, 2008) made this system a possible valid alternative for the creation of a 3-D dataset based on terrestrial or aerial image acquisition systems. These datasets can be useful for the definition of water depth of flooded areas.. 3-D models derived from SfM are nowadays used for geomorphological applications (Westoby et al., 2012) and flood mapping. This second application is often assisted using precise DTM derived from Lidar (Smith et al.,2014; Meesuk et al., 2015, Costabile et al., 2015). Particular applications of SfM can be used to make 3-D models of façades and acquire a useful dataset for the identification of marks left by water. The combined use of low-cost systems able to acquire nadiral images and oblique terrestrial pictures is essential for the

definition of water level and the estimation of damages especially for the flooded area in an urban environment (Griesbaum et al., 2017).

Finally, geolocated photos or information deriving from the internet and social media (Rosser et al., 2017; Fohringer et al., 2015) or by a volunteer geographic information (Hung et al., 2016, Schnebele and Cervone, 2013) can be handy for improving the mapping of flooded areas.

In this work, we present a smart multi-scale and multi-platform methodology developed for the identification and mapping of flooded areas. The methodology has been tested in two areas struck by the flood occurred in Piemonte (NW Italy) in November 2016. The paper presents different case studies that are representative of urban and or not urbanized areas.

2 Study areas

The Piemonte region is located in NW Italy, and most of the territory is inside Po river drainage basin. (Fig 1 A). The Alps range surrounds the region from North to South-west with an elevation higher than 4000 m asl. In the southern sector, Ligurian Alps and Apennines range present lover elevation (1000-2000 m asl) and separate Piemonte from the Liguria sea. On the eastern side, the basin is open to Po river plain. This orographic setting tends to amplify effects of some particular meteorological conditions like severe and slow-moving cyclones located at west of Italy that cause a wet flow from South / East that is blocked by Alps range. This meteorological configuration causes heavy rainfalls especially in autumn when the warm Ligurian sea is a source of additional energy and humidity (Buzzi et al.,1998; Pinto et al., 2013). In the last 30 years, four main floods hit this region: September 1993 (Regione Piemonte, 1996,), November 1994 (Luino, 1999), October 2000 (Cassardo et al., 2013) and November 2016 (ARPA Piemonte, 2016)

In November 2016, a severe flood hit the Piemonte region (NW of Italy). In several areas of Piemonte, in the period 21 – 25 November 2016 different rain gauges registered an amount of rainfall up to 600 mm that represents the 50 % of the mean annual precipitation (Fig. 1 B). The basins of Po and Tanaro rivers were the most affected by the flood that was very similar, for rainfall distribution and river discharge, to 1994 event, which is considered one of the most destructive occurred in last decades (Luino, 1999). This time, the event caused huge damages, activated numbers of landslides and debris flows and caused the inundation of large areas. The civil protection system managed the emergency, and the number of victims was sharply reduced compared to 1994 event that caused 70 victims. The 2016 flood caused a victim in Chisone valley, not far from Torino.

The presented case study area is located in the Po plain south of Turin city (Fig. 1 C). This area is mainly occupied by intensive agricultural activity and urban areas mainly located in the northern part. At the south of Turin, many industrial and commercial areas were built in last decades nearby rivers. From the geomorphological point of view, the actual plain (Fig. 1 B and Fig 1

C) corresponds to the fill of Plio-Pleistocenic Savigliano basin (S.B.), delimited by western Alps, Turin C) Hills (T.H.) and Poirino Plateau (P.P). In the western part, it is possible to find alluvial fans of Chisone, Pellice and Chisola streams (Carraro et al., 1995). The fluvial terraces delimit of actual Po valley with evident relict geomorphology like paleo-meander. The anthropic influence is remarkable with like quarry lake, revetments and embankment that constrain riverbeds (Fig. 1C). The geomorphology is a crucial factor that constrains flooded area shape and the water height.

This area was affected by the flooded of Po River and other tributaries, in particular, Chisola and Oitana streams causing several damages. The Po river between Carignano and Turin stations reached a maximum discharge of 2000-2200 m^3/s in the late evening of 25 November 2016. The mean discharge of this monitoring station in November is 70 m^3/s. The Chisola stream registered a discharge of 200 m^3/s (November average 17 m^3/s) near Moncalieri in the afternoon of 25 November (ARPA Piemonte, 2016).

Inside this area (Fig. 1 C) we focused our attention in particular on two sites were high-resolution data were acquired:

- The village of Pancalieri, located in on the left side of Po river, just after the confluence with Pellice river. In this area it is evident the presence of ancient Po river meanders which were reactivated by the flood with damages to some settlements and destruction of communications roads.
- The town Moncalieri (about 60'000 inhabitants) is located south of Turin in a human-made environment. This area was flooded by Chisola stream on the late morning of 25 November partly due to the collapse of some sections of river embankment. The water interested many residential, service and industrial areas with a maximum water height of 1.5 – 2 m. Another sector of the Moncalieri municipality was also flooded by Po River in the evening of 25 November, with other damages to commercial and industrial infrastructures.

The activation of Copernicus Emergency Management Service (© 2016 European Union) EMSR-192 (http://emergency.copernicus.eu/mapping/list-of-components/EMSR192) allowed to map flooded areas (delineation maps) using Radarsat-2, Cosmo-Skymed and Pleiades images in the most critical areas of Piemonte. In some areas like Moncalieri also a map of damages (grading maps) was produced. However, the available delineations maps represent the automatic extraction of the flooded area at the moment of image acquisition, and generally not at the maximum extension. In the case of Piemonte, they cannot be used for exhaustive modelling and damages evaluations. The preliminary estimate of damages to buildings made by the municipality of Moncalieri is about 50 million of € (M€) for industrial buildings and 13 M€ for residential buildings and others 6 M€ for damages to other goods (http://www.comune.moncalieri.to.it/flex/cm/pages/ServeBLOB.php/L/IT/IDPagina/3669).

3 Materials and Methods

The aim of this study is the definition of a possible methodology for the identification and mapping of flooded areas using low-cost solutions. For this reason, we have combined and compared data from different sensors. We used different approaches for flood mapping some already tested in literature from long time and others more innovative and experimental. We first introduce the concept of 'co-flood' and 'pre/post-flood' data. Co-flood data are collected around the time of maximum inundation while pre/post-flood data are acquired before or after the flood maximum. In the first case, the mapping of flooded areas is more straightforward, but the acquisition of co-flood images could not always be possible.

Using a multi-scale approach, we developed a methodology (Fig. 2) that progressively considers the use satellites and then high and ultra-high resolution systems. The aim is the acquisition of a dataset that can be used to support the identification of water depth and extension reached by the flood. The dataset also allowed making a first evaluation of damages both in urbanized and not urbanized areas

The first identification of the flooded area can be made using satellites results and in situ information coming from the civil protection system that collects reports from local authorities (co-flood phase). This first identification phase is mandatory to have a general and fast indication of the involved area and to plan more detailed acquisitions.

The second phase is aimed to acquire a high definition dataset that can be used for a detailed mapping of the flooded area. For this step is required a system able to fly on demand over large areas and acquire an RGB /multispectral dataset with a resolution of 10-20 cm/pixel. The high-resolution map obtained during this phase can be used for the identification and map of flooded areas with acceptable detail. The resolution of the orthophoto can also support the identification of critical elements like damaged infrastructures: bridges, levees, streets and urban areas involved in the flood. The map of most damaged sectors can be obtained merging civil defence reports and the analysis of acquired orthophotos. The identification of most critical sectors is essential for a preliminary evaluation of occurred damages and the planning of first remedial actions.

On the most critical sectors, especially in urban areas, it is possible to acquire ultra-high resolution dataset (2-5 cm/pixel) that can be used for the quantification of damages or detailed mapping of flood markers. This third phase can be done using Remotely Piloted Aerial Systems (RPAS) or terrestrial systems. This last phase is aimed to quantify the flood severity. In our test, we started from the use of nadiral images acquired by airplane and RPAS, but we immediately realized that in urban areas this approach could be not sufficient for the mapping of flooded limits and the identification of damages. One of the most critical data is the water level reached by the flood that is often visible only on façades of buildings. The identification and mapping of water level markers on façades are mandatory for correct reconstruction of what happened. To obtain a 3D representation of urbanized flooded areas, we decided to integrate terrestrial and aerial images using SfM algorithm.

In the following chapters, we present the acquired datasets of different phases (Table 1). All the proposed systems are low-cost solutions that could be adopted by national/regional Authorities with limited efforts.

3.1 Flood mapping at regional scale with satellite data

The developed methodology is based on a multi-scale approach that starts from the use of low-resolution regional scale satellite images. The use of different available satellites images can support the identification of flood effects at low resolution over large areas and at higher resolution at local scale. The choice of the most appropriate satellite data depends on different factors: i) characteristics of the study area, ii) spatial resolution, iii) revisit time, iv) time of acquisitions respect to the moment of maximum inundation, v) availability and cost of images.

In this paper, only free of charge images were used to assure a low-cost approach. For every considered dataset, we produced a map of the flooded area that represents the synthesis of remote sensing data and geomorphological evidence from 5-m DTM available from Regione Piemonte. We use a visual-operator approach to map flooded areas as resulted more precise than automatic classifications especially in the case of post-flood images. In table 2 are reported the satellite data related to the flood phase. We considered as co-flood data all the images acquired between early November 25 (start of the first inundation) and the evening of November 26, 2016 (withdrawn of water).

3.1.1 SAR data

SAR instruments work in all-weather conditions and in the night time, thus ensuring a high observation frequency and increasing the opportunity to provide data in correspondence at the flood event.

I) Co-Flood mapping. If data are available during the maximum flooding phase, it is possible to accurately map the affected area using high-resolution SAR images as those acquired by the TerraSAR-X (Giustarini et al., 2013) and COSMO-SkyMed (Refice et al., 2014) satellites. In particular, the identification of the flooded area is performed by analysing the SAR backscattering, which shows low values in water-covered areas. In our analysis, we used a SAR image acquired by the X-band COSMO-SkyMed satellites constellation (wavelength ~ 3 cm) on 25 November (05:05 UTC acquisition time). Data has been provided free-of-charge by E-Geos and Italian Space Agency (ASI) in a quick-look preview format with a 60 m x 60 m resolution.

The Cosmo-Skymed data provided is a simple not-geocoded image in grey-scale format (0-255). After the geocoding, we re-classify through GIS software, the SAR amplitude images using empirical thresholds in three main classes: water covered areas (0-60) soil/vegetation (60-160) and urban area (160-255). The investigated area is almost flat, so it is not affected by

problems related to geometrical distortions of backscattering. The validation of the classification accuracy was made by comparing the reclassified image with an aerial photo, optical images, and land-use database. The analysis with such data points out the relevance of co-flood images for fast mapping of flooded areas. We remark that it is not possible to know a priori if a co-flood image will be available during the maximum of the flood event. However, the short revisit times achieved by the new generation of SAR satellites can significantly increase the possibility to collect co-flood data.

II) Post-flood mapping. We also performed a post-flood mapping by exploiting data acquired by the Sentinel-1 mission which is composed of a constellation of two satellites, Sentinel-1A and Sentinel-1B, launched on 2014 April 3, and 2016 April 25, respectively. Sentinel-1 satellites have been designed to acquire C-band SAR data in continuity with the first-generation ERS-1/ERS-2 and ENVISAT mission, developed within the European environmental monitoring program, Copernicus. The Sentinel-1A SAR operates at 5.405 GHz and supports four imaging modes providing images with different resolution and coverage (Torres et al., 2012). We used the Interferometric Wide Swath Mode (IW) acquisition mode by employing the Terrain Observation by Progressive Scans (TOPS). The IW TOPS mode is the primary mode of operations for the systematic monitoring of surface deformation and land changes (De Zan and Monti-Guarnieri, 2006). This acquisition mode provides large swath widths of 250 km with a spatial resolution of 5 m × 20 m (IW). The repeat cycle of the twin Sentinel-1A/B constellation is reduced to 6 days.

For our analysis, we have acquired two IW Sentinel-1A/B images collected over the study area, in VH polarization along the descending satellite passes. In particular, we have exploited data acquired after (on November 28, 2016) and before (November 22, 2016) the flooding event (see Table 3).

SAR data, provided in the Single Look Complex (SLC) format, has been first radiometrically calibrated to convert the digital number (DN) values into corresponding backscattering coefficients, i.e., sigma naught (σ^o) values, which contain information on the electromagnetic characteristics of the surface under investigation. Subsequently, calibrated SAR data have been multi-looked with one look in the azimuth direction and four looks in the range one, and finally geocoded, by converting the maps from radar geometry into Universal Transverse Mercator (UTM) coordinates (zone 32T).

After these pre-processing steps, to detect land surface changes induced by flooding, we have computed the difference between the post- and the pre-flooding geocoded backscattering coefficient images, and produced the map of the temporal variation of the surface backscattering ($\Delta\sigma^o_{\text{post-pre-flooding}}$).

3.1.2 Multispectral satellite data.

In this category, we considered both low and medium resolution images. Unfortunately, we found co-flood images only for low-resolution images.

I) Medium-Low resolution satellite data. MODIS (Moderate Resolution Imaging Spectroradiometer) is a system of two sun-synchronous, near-polar orbiting satellites called Aqua and Terra that daily acquire images all over the World (Justice et al., 1998). Terra acquires images in the late morning while Aqua in the early afternoon, satellites also have a night time pass when they acquire in the thermal bands. This repeat frequency does not occur along the same ground track, and the repeat cycle along the track is every 16 days. The high revisit time allows detecting with more probability flood over vast areas when they still flooded and not covered by cloud. We searched for first free-cloud MODIS images from Earthdata portal of NASA (https://worldview.earthdata.nasa.gov; The selected image was acquired by Aqua satellite on 26 November 2016. We used the 6-bands products with a spatial resolution from 250 to 500 m that range from visible to near-infrared (NIR) and shortwave infrared (SWIR) (Table 4). For the elaboration, we used the MYD09 - MODIS/Aqua Atmospherically Corrected Surface Reflectance 5-Min L2 Swath 500m, (Vermote, 2015) downloaded from http://ladsweb.nascom.nasa.gov/). To have a benchmark of the non-flooded situation, we also used the Aqua satellite image of 12 November 2016, which was compared with the image taken during the flood. We did not apply an atmospheric correction to images because the MYD09 product is adequate our aim. Moreover, the study area is small (20 km) and the atmospheric parameters for correction available at 1 km of spatial resolution (water vapour, ozone or aerosol) don't show significant change. For the identification of flooded areas, we make the following elaborations:

a) False colour image made with combinations of 7-2-1 bands for a visual interpretation of flooded areas;

b) Modified Normalized Difference Water Index variation $MNDWI_{var}$ (Equation 1). The MNDWI allow detecting water masses or soil moisture. In literature, different combinations for this index are presented and discussed (Xu, 2006; Zhang et al., 2016; Gao, 1996). In our study, we used the ratio between B1 (red band) and B7 (Short Wavelength Infrared - SWIR). The difference with a non-flooded situation can be used for identifying changes in soil moisture. We used the results of supervised classification to mask the cloud cover.

$$MNDWIvar = MNDWIpost - MNDWIpre \qquad \text{where } MNDWI = \frac{(B1-B7)}{(B1+B7)} \quad (1)$$

c) Supervised classification of co-flood image. Supervised classification has already been used in literature to map flooded areas, using machine learning, as described in Ireland et al., (2015). In our work we made a simple supervised classification with SAGA GIS. We first manually defined the training areas with main land use typologies visible on the false colour image. We try different methodologies for the classifications and we chose as most accurate the

maximum likelihood with absolute probability reference and spectral angle methods. We validate the reliability of these classifications with a comparison with false colour image and land-use database. Then, using a GIS query, we extracted the category "area covered by water or wetland" that mostly correspond to the flooded area for accuracy statics reported in result chapter.

II) Medium-high resolution satellite data. Medium-high resolution multispectral satellites (e.g., Sentinel-2 A and B or Landsat 8) have a longer revisit time (from 5 days for the Sentinel-2 constellation to 16 days for Landsat-8) and it is more difficult to have images at the same time of the maximum flood and cloud free. However, by comparing two images acquired before and after a flood event, it is possible to calculate the variation of different indexes related to change in reflectance of the soil or/and of the vegetation. In this way, it is sometimes possible to map the flooded area indirectly (post-flood mapping). In our study area, we used images taken by Sentinel-2 before the flood (2016, November 11) and after (December 1). Sentinel-2 has some bands at 10-m of spatial resolution and some bands and 20-m of spatial resolution resumed in Table 5. To detect flooded area, we first made a visual interpretation using images with different bands composition of post-flood data. The comparison of considered images allowed calculating the difference between two indexes:

1. The Normalized Difference Vegetation Index (NDVI) variation. The NDVI calculated with 10 m of spatial resolution images Sentinel-2 using the near-infrared band (NIR - B8), and the red band (B4). The NDVI is related to the activity of vegetation, and it is possible by calculating its variation (equation 2) to identify the decrease of NDVI values as an effect of inundation on vegetation (Ahamed et al., 2017). The detection of this change allows mapping flooded areas indirectly.

$$NDVIvar = NDVIpost - NDVIpre \qquad \text{where } NDVI = \frac{(B8-B4)}{(B8+B4)} \qquad (2)$$

2. The Modification of Normalized Difference Water Index (MDWI) variation. We use a similar index already tested for MODIS data. We used Sentinel-2 to calculate the MNDWI considering the red edge band (B5) and the SWIR band (B11) at 20 m of spatial resolution. With this approach (equation 3), it is possible to map the variation soil moisture related to recently flooded areas or areas that are still covered by water.

$$MNDWIvar = MNDWIpost - MNDWIpre \qquad \text{where } MNDWI = \frac{(B5-B11)}{(B5+B11)} \quad (3)$$

3.2 Flood mapping at local scale with high and ultra-high resolution data

The flood mapping at local scale was made using high and ultra-high resolution images.

Immediately after the event, a research project proposed by CNR-IRPI was conducted with the participation of ALTEC S.p.A., Digisky s.r.l. and the Civil Protection Agency of the Metropolitan City of Turin. The aim of the project is a methodological analysis of a possible low-cost solution that could be used for high-resolution mapping of flood effects.

The study started from SMAT F2 Project results (Farfaglia et al., 2015), where different solutions for the acquisition of RGB datasets with small and medium Remotely Piloted Aerial Systems (RPAS) were developed. Also previous experiences of CNR IRPI and Civil Protection Agency in the use of small RPAS for the study of geo-hydrological processes (Giordan et al., 2015; Boccardo et al., 2015; Fiorucci et al., 2017; Giordan et al., 2017) were useful for the definition of a correct use of these systems. These previous experiences pointed out how the use of low-cost systems for the acquisition of RGB images and the application of structure from motion algorithm (SfM) can be considered a good solution for the creation of high-resolution 3D models.

3.2.1 Aerial high-resolution images

Aerial photo took few hours or within few days after the peak of inundation allow mapping the flooded area with high precision over the most involved territories. In our case, aerial photos were acquired after the flood over the Po river near the village of Pancalieri and for Moncalieri town. We used a low-cost aerial platform (Tecnam P92-JS) provided by DigiSky s.r.l. equipped with Panasonic Lumix GX7 camera (mirrorless with 16 Mp) that allowed to acquire aerial photo with a spatial resolution of 10 cm/pixel. The system also has an onboard GPS that acquires images shooting points and allows the georeferencing of the photos sequence using SfM.

The use of manned solution has several add values that can be very useful in this phase: i) it is possible to fly over urban areas without strong limitations that characterized RPAS; ii) the system can acquire images over large areas in a limited lapse of time; iii) the system can flight on demand during the flood or immediately after (with favourable weather conditions).

The adopted solution was used to acquire 9.2 km^2 of the most damaged area of Moncalieri and 9.5 Km^2 of the flooded area of Pancalieri. These two areas are representative of different conditions:

1) The area of Pancalieri is a rural area mainly dedicated to the agriculture. In this case, the Po river flood covered large uninhabited sectors of the Pancalieri plain and reached part of the town of Pancalieri. Here, using SfM, the images of the plane were also processed for the creation of a DSM (resolution of 20 cm) with the aim of mapping geomorphological features related to the flood.

2) The selected area of Moncalieri is a strong urbanized sector of the municipality. In this area there are: i) a motorway, ii) several regional and local streets iii) a residential area with recent unfamiliar houses and small condominiums, iv) an industrial and commercial district. The inundation of this area is due to the Chisola levees breaks. The map of Moncalieri was useful for

the identification of most damages elements and in particular the levee. In the most critical areas, we also used RPAS to acquire ultra-high resolution images.

3.2.2 RPAS ultra-high resolution images

The ultra-high resolution phase is based on the use of RPAS and a terrestrial system. RPAS were used to acquire nadiral photo sequences of the most damaged areas and infrastructures. In particular, we tested the possibility to use RPAS for the identification of damages occurred to the Chisola river levee and one of the most damaged sectors of Moncalieri town. The employed RPAS is a multirotor (CarbonCore 950 octocopter) equipped with a Canon EOS M (Sensor CMOS APS-C, 18Mp). The system is equipped with a flight terminator and a parachute and can also be used in inhabited areas. Civil Protection Service of Turin metropolitan area provided RPAS. The obtained aerial photos have a spatial resolution of 3 cm/Pixel. Using SfM, the images of the drone were also used to create 10 cm resolution DSM. All the flood mapping methodology described until now are very often not able to give a consistent measure of water depth. This limitation is not due to the resolution or the time of acquisition, but it is intrinsic in nadiral images. For this reason, in Moncalieri area, we choose to deploy a ground-based solution.

3.2.3 Ground-based ultra-high resolution images

As mentioned before, we tested a low-cost terrestrial system for the acquisition of ultra-high resolution images. In particular, we used an integrated system developed by ALTEC SpA, which couple a Go-Pro HERO 3+ (Black Edition) camera with a GPS and an acquisition module. The system is able to record a STANAG 4609 geolocated HD video. The experimental system was installed over a CNR IRPI car, and a survey was done few days after the flood in the considered area of Moncalieri. The continuous record of geolocated video can be a good solution for the acquisition of a significant amount of data immediately after the flood when marks of the water level are still clearly visible along building facades. The identification of water level of flooded areas based on the measurement of marks over facades is not a novelty, but the manual acquisition of these data has often been a critical task. Citizens often want to quickly obliterate these signs as a reaction to the critical experience that they lived. The use of field teams that look for these marks can be a time-consuming task that can produce few results with considerable efforts also because before the survey it is hard to have an idea of the number and the distribution of facades marks that can be identified and measured. The number of marks strongly decreased after few weeks, and for this reason, it is essential to have a system that can acquire very fast geolocated images and that can be easily used over large areas.

The presented system is straightforward and efficient. The geolocated video can be analysed by other components of the team immediately after the acquisition or after many days. The primary goal is the fast acquisition of numerical information of the flood effects that can be used for several purposes. For the identification and mapping of water levels, the video is analysed, and a frame sequence is extracted from it when the operator sees some marks lefts by water over facades. The developed system can extract not only frames but also their geocoding information, which are computed using SfM applications. The result is a georeferenced 3D model of the façade that can be used to measure the water level with a good approximation (few cm). We validate the accuracy measures of water level based on SfM with manual measures accurately geolocated with GPS RTK positioning.

3.2.4 Field data

Field survey, ancillary data like a measure of river discharge stations, and civil protection reports were used to validate the maps derived from remote sensing interpretation and the simulation models for Pancalieri and Moncalieri areas. We made a GPS RTK campaign in Tetti Piatti and Tagliaferro areas to have direct measurements of flood marks. In particular, we acquired the 3D position of marks previously identified using the available video. We used third part materials like newspaper reports, photo and videos found on the web with a validation of their reliability regarding geolocation and time. Available data were used to check the extension of flooded area and water height mapped with other methodologies.

3.3 Water depth models based on DTM approach.

As mentioned before, the primary goal of the presented methodology is the definition of the maximum depth reached by the water during the flood. The map of water maximum depth (WD) is an important document that can be used for the first definition of damages and remedial actions. All the acquired material, and in particular data that define the water depth reached by the flood, were used to calculate the water maximum depth map. In our study, we adopted a simple raster-based model (Bates and De Roo, 2000) and we created an absolute water level (WL) raster. The first step is the acquisition of several measure points of water level (WL_p) that are calculated from the measured water depth point (WD_p). WD measures can be done using: i) georeferenced photos (low accuracy); ii) ultra-high resolution measure derived from SfM and integrated with manual measure geolocated GPS RTK positioning (high accuracy); iii) civil protections reports (the level of accuracy can be very different); iv) data acquired by hydrometric river level monitoring stations. Starting from the collected spotted measures and the 5-m LIDAR digital terrain model (DTM) freely provided by Regione Piemonte, we calculated the WL value for each

point using a simple formula: $WL_p = DTM + WD_p$. Available WL points were used to create the water level contour lines and then interpolated using GIS software to obtain the raster of WL gradient. The WL raster is used to create the raster map of water depth which can be calculated with a simple raster calculator of GIS software using the reversed formula WD=WL-DTM. WD map is necessary information to assesses and improve the limit of the flooded area and, it is also fundamental for the phase of preliminary damages assessment. We produced maps of water depth at medium resolution for Po river (Fig. 5) and high resolution for Moncalieri (Fig. 11) and Pancalieri area (Fig 6).

4 Results

4.1 Flood mapping from low to medium-high resolutions with satellite data.

The satellite data allowed mapping the flooded areas by Po river, Chisola and Oitana stream, with a resolution that ranges from 500 m of MODIS to 10 m of Sentinel-2. In following figures (Fig.3. Fig 4. and Fig.5), raster maps based on remote sensing data are compared with our perimeter of the flooded area (black polygon). We manually extrapolated the flooded area perimeters considering both satellite data and geomorphological features observed in the hillshade model derived from 5-m DTM of Regione Piemonte. For the evaluation of automatic flooded area maps based on satellite data, we applied a GIS query for each map to create boolean rasters of flooded / not flooded area. Then we overlapped the obtained raster with manual polygons for a geo-statistical analysis, for each polygon is reported the percentage pixel classified as flooded/not-flooded. The main results are reported in table 6.

For Po and part of Chisola, the flooded areas were also mapped with the help of WD model based on DTM. At the moment of writing this paper (November 2017), it is still not available an official delimitation of flooded areas, a map made by ARPA Piemonte is under validation, and the data will be published in the next months.

4.1.1 Flood mapping with SAR data

I) Co-flood mapping, the reclassified amplitude of COSMO-SkyMed data. Results of image classification are shown in Figure 3A, where three classes of SAR amplitude were defined by means of empirical thresholds: i) low that correspond to water covered area (blue); ii) intermediate like soil/vegetation (green); iii) high that are urban areas (pink). In the figure are also overlapped the quarry lake from ancillary data (cyan). The accuracy in the correct detection of land-use type is quite good ranging from 80 % for soil and vegetation, 67% for urban area to 61% for water body (tested in quarry lakes). Vegetation and buildings are factors that reduce the detection of water covered areas even using full-resolution images and more complex

processing (Pierdicca et al., 2018). In a second step we selected with a GIS query the low resolution (water covered) class that mostly correspond to the inundated areas and we compared with the real flooded area. Also the accuracy in the correct detection of flooded areas is quite good: it ranges from 57 % in the lower Oitana stream to 2% in the Po area near Moncalieri. This is related to the time of satellite acquisitions (05:05 UTC of 26 November 2016) some hour before the flood peak. The flood wave positions can be appreciated especially along the Po river, where upstream (near Pancalieri) about the 42% of the flooded area was detected, while downstream (Carignano) decrease to 4%. The urban area of Moncalieri limits the capability detection of inundated areas. The false positive errors are less than 5% of the area.

II) Post-flood mapping with Sentinel-1 data. Figure 3B shows the map of the post- pre-flood SAR backscatter difference ($\Delta\sigma^{o}_{post\text{-}pre\text{-}flooding}$) where the application of empiric thresholds allowed us detecting areas covered by water, i.e., flooded ($\Delta\sigma^{o} <$ - 1dB). Such results show that most of the areas classified as flooded by the co-flood analysis were not anymore covered by water on 28 November 2016. Only small depressed areas, e.g., ancient meanders of Po river, were still flooded, as shown in Figures 3D', 3D'' and 3D''' (the case of Pancalieri, discussed more deeply in par 4.2.).

4.1.2 Flood mapping with multispectral data

I) Multispectral low resolution, MODIS-Aqua. The MODIS-Aqua satellite took an image reasonably free of clouds over the entire Piemonte during the late morning of November 26, 2016. The image allowed detecting the flooded areas with a resolution of 500 m.

From the false colour images (Fig. 4 B), even if the area at the south of Turin is not yet directly flooded, it is only possible to detect that the soil was saturated of water (dark green-blue in false colour composition). The comparison with pre-flood image of November 12, 2016 (Fig. 4 A) improved the detection of the flooded area.

We also try to extract in an automatic way the flooded area with the equations previously described:

In figure 4 C we identified flooded area using a GIS query with the value $MNDWI_{var} \geq 0.3$. This value is an empirical threshold that allows selecting most of the flooded area and minimizes false positive errors. The results show a good correspondence between the manually drawn and the automatically classified flooded area, however around 35% of the flooded area was not identified. The mismatch can be explained with the satellite acquisition at the end of the co-flood stage when water started to withdraw. It is also possible to see some false positive pixels (<10 %) that correspond to the shadow of the clouds or haze that was not possible to entirely filter.

Supervised Classification. We also made a supervised classification of 26 November MODIS image using maximum likelihood (MLC) (Fig. 4 D) and spectral angle (SA) (Fig. 4 E) methods. In the study area, we classified, four primary land cover:

vegetation, bare soil, cloud, and water body / wet soil that almost identify the flooded sector (the water bodies likes the quarry lakes are too small for MODIS pixel). After a visual checking of the classification reliability, we used a GIS query to select the "water covered and wet areas" classes. The query creates a boolean raster of flooded areas. The accuracy of flood map based on supervised classification is good: it identifies most of the flooded areas for Po river (> 70 %) with low false positive pixel (table 6). Worst results for the are flooded by Chiosla and Oitana.

For both indexes, it possible to see that the town of Moncalieri (red square 1 in figure 4) flooded by Chisola stream is not well identified.

II) Multispectral medium-high resolution post-flood mapping Sentinel-2. The images of Sentinel-2 were analysed by visual interpretation of RGB composite image and using two different indexes (NDVI – MNDVI) to identify flooded areas shown in figure 5. For both indexes we used GIS queries with empirical thresholds to extract the flooded area:

1) NDVI variation ($NDVI_{VAR}$) at 10 m of Spatial resolution (Fig. 5 A). The results show that for Po, Chisola and Oitana a clear pattern of negative NDVI variation corresponds to the flooded area. The study area is almost flat and mostly occupied by cultivated fields and, in November, it was characterized by tillering of wheat. The flood caused a deposition of a thin layer of silt sediment that caused a decrease of vegetation activity (most of the flooded area shows an $NDVI_{VAR}$ <-0.06) that could be detected using the available dataset. By the contrary, the wheat field outside flooded area shows an increasing or stationary NDVI. In the maps are visible negative $NDVI_{VAR}$ also outside the flooded area that is related to: i) winter decreasing of activity of natural vegetation or some cultivations, ii) longest building shadow in urban areas. The presence of false positives hampers the use of automatic classifications of flooded areas, and a visual interpretation is necessary. It is possible that flood effects and the layers of silts could have also affected the crop productivity with relative economic damages as reported in other cases (Tapia-Silva et al., 2011; Shrestha et al., 2017), but this evaluation is not the aim of this study.

2) MNDWI variation ($MNDWI_{VAR}$) at 20 m of spatial resolution. The index is directly related to the presence of water or high soil moisture. The results show that for Po, Chisola and Oitana floodplain (Fig. 5 B) a clear pattern of positive $MNDWI_{VAR}$ that indicates an increase of soil moisture and the presence of some areas that were still inundated. It is possible to see that a threshold of $MNDWI_{VAR}$ + 0.1 is the best to delimit the flooded areas. However, like for NDVI, the presence of many areas with positive variations outside the flooded sector makes more accurate a manual interpretation compared to an automatic classification. The evidence also suggests that for this index it is important to have images taken within few days after the flood when the affected areas are still covered by water or with soil very wet. In table 6 are resumed the accuracy statistic for automatic mapping of flooded areas based on satellite data: MNDWI show little better accuracy than NDVI. It is worth to note that for both $MNDWI_{VAR}$ and $NDVI_{VAR}$ the flooded area is well detectable in the around the village of Pancalieri (> 50% of

accuracy) where land use is mostly cultivated land. On the other hand, is more difficult to detect the flooded area in the high urbanized town of Moncalieri (<20% of area detected).

III) Water depth model. We create WD model for Po river following the procedure described in paragraph 3.3. The results are shown in figure 5C. The simulated WD model has a good match with benchmark polygon and the evidence from Sentinel-2 (Fig. 5 A and B), MODIS data (Fig. 4). It is also possible to observe some discrepancy at South-East of Moncalieri where large area should be flooded according to model but in reality, was not affected. This mismatch could be explained by the presence of artificial structures (e.g., embankment) that protect flood-prone areas and our model cannot simulate. The uncertainty of our WD model is complicated to evaluate because it depends on many factors: the main limits is the number of ground-based WD measures, their reliability and their geolocation. The interpolation to obtain water table is also another source of error. The Lidar DTM of Regione Piemonte accuracy in elevation is range from +/-0.3 m to +/- 0.6 m in urban areas. Over this vast area we have not ground measure for validation, but it is possible to estimate from some photos found on the web that model error is about 0.5 m. In the high-resolution WD model of Pancalieri and Moncalieri shows in the next chapter was possible to validate data with ground truth evidence.

The final limits of the flooded area are the results of both remote sensing and WD model interpretation. Its accuracy can be considered acceptable for large cultivated and flooded area by Po river but less accurate for urban zone especially in Moncalieri where a local high-resolution analysis is needed to quantify the severity of the flood.

4.2 Flood mapping at local scale with high-resolution data.

Inside the area analysed using remote sensing systems, we choose the most critical sectors of Moncalieri and Pancaleri to test high and ultra-high resolution images. As mentioned before, the high resolution has been acquired using an aircraft, the ultra-high resolution using RPASs and a ground-based photosystem. All the images have processed using SfM that allowed to obtain orthophoto and 3D models.

4.2.1 High-resolution aerial photo, Pancalieri

Po river partially flooded the village of Pancalieri on the morning of November 25, 2016. This area has also been mapped by high-resolution aerial photo (10 cm/Pixel, RGB bands) provided by DigiSky. Aerial photos were taken November 28, 2016 (figure 6 A) and allowed to refine the map of the flooded area form the medium resolution maps obtained with the interpretation of Sentinel-2 data. With the help of digital surface models (DSM) at 0.2 m of spatial resolution derived from SfM, we also mapped geomorphological features like erosion (meanders cut) and deposition areas and road damages (Fig. 7 C). The

integration of aerial photo and DSM also allowed making a 3-D model where it was possible to measure water depth for some points where water level marks are well detectable (Fig. 7 B).

Using the procedure described in paragraph 3.3 we produced a WD model for the Pancalieri area (Fig. 6 D) with higher accuracy respect to the rest of Po valley. The higher accuracy of the model was obtained using: i) high-resolution aerial photos ii) spot measures derived from SfM iii) different video and photos found on the web and geolocalized with the help of Google Street view (e.g., Fig. 6 B and 6C). The model shows that part of the Pancalieri village was flooded by a modest height of water (< 0.5 m) while near Po river WD reached 2-3 m with a fast flow that caused erosion channel. From the map of the flooded area (Fig. 6 D) it is also interesting to note that, during the flood, ancient meanders at the east of Pancalieri were reactivated and ad consequence some areas were flooded quite far from Po main course.

Some months after the flood (April 2017), satellite photos available on Google Earth (0.5 m spatial resolution) still show some trace of flood like erosions and area covered by sand deposits. The flooded area is much more difficult to identify and confirm the importance to acquire data as soon as possible after a flood event.

4.2.2 High-resolution aerial photo and ultra-high resolution RPAS 3D models, Moncalieri.

Some parts of Moncalieri municipality (Tetti Piatti, Carpice and Tagliaferro localities) were flooded in the late morning of 25 November by Chisola stream that breached its embankment in different points (Fig. 8 B). On the left side of Chisola, the area with a very dense residential and industrial settlement suffered severe damages. Hundreds of people were evacuated. In the evening of November 25, Po river flooded another sector of Moncalieri municipality.

Few days after the flood, the area flooded by Chisola was analysed with different methodologies:

1. High-resolution aerial photos. Like in Pancalieri, on November 29 a very high resolution (0.1 m/pixel) aerial photo using the aerial platform of DigiSKY was taken over an area of about 9.2 km^2. The aerial photo allowed to refine the map of flooded areas (Fig. 8 A) and to detect the points where river embankment collapsed (Fig. 8 B).

2. Ultra-high resolution RPASs photos. On December 3, 2016, RPAS acquired photos (resolution of 0.02 / 0.03 m/pixel) over some most critical areas (e.g., Tetti Piatti – Fig. 8 C) for precise mapping of flood effects. In this area, ultra-high resolution allowed to detect some damages like the toppling of a wall in recently built urbanization or the waste accumulation derived from damaged objects initially located in houses or industrial warehouse. The presence of these deposits is a clear evidence of the occurred damages, but also a confirmation that nadiral images are not able to supply a sufficient dataset for the identification and evaluation of damages in urban areas.

The DSM based on RPAS photos also allowed to create a detailed 3-D model of river embankment rupture (Fig. 9). The presented 3D model confirmed that the level of Chisola during the flood was very critical with a difference of fewer than 0.5

m from the top of the levee. The maximum water level considered under the security limits suggested by Po river authority is 1 m concerning the top of the embankment. The RPAS model also allowed to map geomorphological effects of the rupture of the embankment. In particular, figure 8B and figure 9 show a massive erosion of field near the break and a pseudo alluvial fan created by the flow of water.

490

4.2.3 Measure of water depth with SfM model from terrestrial camera, Moncalieri.

In the same days of UAV an aerial photo campaign, a field survey using an integrated system provided by ALTEC S.p.A. installed on a car (Fig. 10 B) was made in the same urban areas of Moncalieri flooded by Chisola (Fig 10A). The survey had the aim of measuring the maximum water level reached and made a rapid evaluation of damages. The survey last about 1h for
495 12 km of the path along the road of the most critical area hit by the flood.
Where the level reached by the water was still visible over several facades, (Fig. 10 C and Fig.10 D) it was possible to estimate the maximum water level of the flood. During the first survey, we found 11 points where watermarks over facades were still visible. During the post-processing, we realized that the quality of the images extracted from the video was insufficient for the SfM application: the bitrate was too low and the frames are too pixelated. For this reason, after a month we performed a second
500 survey with a higher bit rate along the same path, but only six marks still visible (Fig 10 A). This reduction of available points confirmed that the delay between the flood and the survey is a fundamental element that should be carefully considered because the number of possible information decrease exponentially. For this second terrestrial camera acquisition, an improvement of the encoding quality was introduced. Such improvement allowed the extraction of high quality images compatible with SfM application. We obtained 3D models of the surveyed sectors, and we measured the high of water marks on façades. Then we
505 validated the information obtained from SfM with a manual water height measurement geocoded with GPS RtK systems for the 6 points and other additional 5 points. The accuracy of measurement considering that is a low-cost solution and one of the first experimental tries for this system is excellent: the average error compared SfM water level measurement with manual measure can be estimated in few centimetres (see table 7).

4.2.4 High-resolution water depth models and ancillary data for damages evaluations, Moncalieri.

510 The combined use of measures derived from: i) car camera elaborated with SfM, ii) manual GPS RTK, iii) the hydrometric level of Chisola stream registered by ARPA Piemonte station (Fig. 11 B) represents a useful dataset for the estimation of the WD. Using the 5m DTM Lidar of Regione Piemonte, we obtained the WL and the WD rasters (Fig. 11 A). The result shows that in large part of the analysed area, the water height was between 0.5 and 1 m. Unfortunately, in some morphological

depressions, the level was higher than 1.5 m. The model also shows that in the cultivated area close to left Chisola embankment water probably reached 2 -3 m height.

The water level map can suffer from some errors from spot measure. These are related to the quality of DTM or the effect of local structures that can modify the water flow and height at a local scale. The comparison of water level measured with SfM / GPS and calculated level with DTM show variation within 0.2 m that is a good result (Table 6).

Ancillary data like photos or video found on the web (local newspaper, social media) and geolocated with Google Streetview allowed to improve and validate the map of flooded areas and the height of the water (Fig 11 C). On the web, it is possible to find a lot of photos or video of the flood event, but only small part of them can be geolocated with adequate precision and validated.

The water height map was crossed with buildings database of Regione Piemonte to assign to each building the average of water height reached by the flood (Fig 12 A). The water height is one of the leading parameters that can be used for a preliminary estimation of potential damages. We dived the water height in 3 main classes corresponding to low (<0.5 m), medium (0.5 – 1.5) and high (> 1.5) damages expected. These thresholds have been empirically defined by Luino et al., (2009) and Amadio et al., (2016). The obtained map is a good representation of the level of damages caused by the flood that could be considered the final product of the presented methodology.

This result was compared with ground data where possible: for instance, in the industrial warehouse shows in detail map in figure 12 B was estimated an average value of 0.8 m water level (medium degree of damage expected). The evidence from a geolocated photo from La Stampa newspaper confirms this value.

4.3 Flood mapping strategy flowchart

The flowchart in figure 13 shows the approach that we purpose for the choice of instruments and methods to map the flooded areas, based on the results of this study. If free satellite data are available, it is possible to sort them taking into account the parameters of time elapsed from flood and the spatial resolution:

I) The priority is to search for co-flood images that allow an easy mapping. In case of night and cloudy conditions it is necessary to use SAR image (Sentinel-1) while for multispectral data acquired during the day the choice is related to spatial resolution: for instance, Sentinel-2 or Landsat-8 data are more resolute than MODIS data.

II) In the case we have post-flood satellite pass only multispectral data can be used. Also for post-flood data, the spatial resolution and time elapsed from the flood are the parameters that should drive the choice. The use of post-flood data implies more complicated post-processing (e.g., bands index variation) and with the support of ancillary data and DTM to extract the

flooded area map. In general, the rapid access to data portal of free satellite data allows to download the data and to make an evaluation of the best solution for the case under study, that not necessarily is the data with high spatial resolution.

After this step it is possible to make the first delimitation of flooded areas, that in case good data may be an already corrected and ready to use map. Then it is possible to focus the acquisition of on-demand of high-resolution sensors only in the most critical or unclear areas (case 2A). If we use only on-demand data, without rapid satellite mapping, we could map large area at high spatial resolution (case 2B). This solution, however, implies a higher cost. In case of direct mapping at very-high resolution, it is better to use low-cost aerial platforms that are more flexible respect to on-demand commercial satellites. The integration with DEM data allows creating the water depth model at basin scale and a further refinement of flooded area maps (2C).

Urban area flood mapping (3) can be considered a hotspot priority inside the general flood map. It needs a more accurate and high-resolution mapping with use of ground-based measures (like SfM model based on car photo), RPAS survey, and the creation of a water depth model that is essential for a precise flood magnitude assessment.

It is important to remind that is not possible to select a priori which type of data/processing is the better for flood mapping. The best method to use depends on different factors: 1. Satellite acquisition and time elapsed from flood peak; 2. Type of satellite data (SAR / multispectral, spatial resolution); 3. Study area features and risk (dimension, cloud cover, land-use and element at risk); 4. Affordable cost (e.g., we use commercial satellite data or traditional aerial photo only if they give significant advantages to flood mapping)

5 Discussion and conclusions

In this work, we tested different methodologies for a low-cost and rapid flood mapping and water depth assessment using the November 2016 Piemonte flood as a case history. We used a multiscale and multi-sensor approach to know pros and cons of each methodology about the site conditions and available data. We also proposed a flowchart model to map flooded areas from satellite to ground-based data,

At the regional scale, satellite remote sensing showed a good performance in the flood mapping: the combined used of SAR data of Sentinel-1 and Cosmo, and multispectral data of MODIS-Aqua and Sentinel-2 allowed creating maps of the flooded area. The maps of flooded areas automatically extracted from remote sensing data were used with the help of DTM and water depth model as a base map for an accurate manual drawing. In our study area (320 km^2) about 66 km^2 was flooded by Po river, Chisola and Oitana streams. WD models show that some areas were flooded up to 2 m of water height.

Concerning SAR data, we reclassified a simple preview low-resolution Cosmo-Skymed amplitude image acquired some hours before the co-flood time. The results show that the time of satellite pass is fundamental: if the area is covered by water (like upstream part of Po river) up to 60% of pixels was correctly classified as flooded and it was possible to observe a definite pattern. We compared pre- and post-flood SAR images of Sentinel-1 making SAR backscattering difference of radiometrically calibrated images. The result shows that SAR is weaker for post-event mapping: in our case 3 days after the flood (Sentinel-1) less than 4% of the flooded area is still detectable. By considering the obtained results, it is also clear the importance to have free and constant SAR satellite data provided by national agency: a short revisit time and a constant acquisition are factors that increase the probability to have SAR image for real-time flood mapping. For instance, the two Sentinel-1 provide free images every six days, while other satellites have quite high costs and the acquisition of the extra images is activated with emergency procedure acquisition like the EMSR of the European Union or by civil protection authorities.

The low-resolution MODIS image acquired near the co-flood stage allowed a good identification of flooded areas using different methods: MNDWI variation and supervised classifications. The detection accuracy is good especially for the area flood by Po river where about the 70% of the flooded area was correctly identified.

Medium-High resolution multi-spectral data have more capability with post-event images. In this work, we tested NDVI and MNDWI variations for the detection of flooded areas based on the comparison of pre- and post- event images. Both methodologies show quite good performance in cultivated land, (40 % - 45% of accuracy). Here it is possible to detect a clear pattern: inside the inundated area the percentage of pixel classified as flooded is four times greater than in not flooded area. The inundated areas are more difficult to detect in the dense urban area of Moncalieri (only 4% area was correctly mapped). Water depth model and DTM gave an important help in the improvement of flooded area of Po river based on remote sensing data. In last years, the revisit time for free multispectral data was sharply reduced (Landsat-8 has a revisit time of 16-days and Sentinel-2 of 5 days from March 2017 with the launch second satellite). This increase the probability to have an image free of cloud within few days or weeks after the flood or in some cases during the inundation phase. At the local scale, flood mapping showed a good agreement with regional scale mapping.

The high-resolution aerial photo and ultra-high resolution aerial photo from RPAS allowed mapping flooded areas with more precision. The application of Structure from Motion (SfM) allowed creating high-resolution DSM useful to map the geomorphological effects (e.g., meanders cut) and the widespread damages (embankment rupture) in Pancalieri and Moncalieri area.

In the urban area of Moncalieri, where satellite data have low accuracy and precise evaluation of water depth is necessary for flood damages evaluation, the solution is the integration with ground-based data. In our work, we tested a low-cost solution with a GO-PRO HERO 3+ (Black Edition) camera installed on a car that allowed to make 3D models and to measure the water

height reached during the flood. These measures validated with GPS showed good accuracy, but it is necessary to do the survey within few days after the flood when many water signs are visible. A proposal for the future is to use this system during the emergencies, for instance, on civil protection car, to have a map of water depth with a much higher density of points.

Using these measures and a high-resolution DTM, it was possible to generate a raster model of water depth that has a good match with the ground truth about +/- 0.2 m of accuracy. We used the results of WD model for a preliminary evaluation of building damages. The model could also be used in the future for flood prevention policy or civil protection plans.

Finally, from our work it is also clear the importance to collect ancillary data also from the new sources on the web: the photo and video collected during the flood by simple citizens can be a precious help for the validation of flooded area maps.

Data availability.

MODIS data were downloaded from NASA LAADS - DAAC portal (http://ladsweb.nascom.nasa.gov/) link retrieved 30-03-2018

12/11/2016: MYD09.A2016317.1215.006.2016319043220

26/11/2016: MYD09.A2016331.1225.006.2016333031908

Sentinel data were download from Copernicus Scihub: https://scihub.copernicus.eu/ link retrieved 30-03-2018

Sentinel-2:

1/12/2016: S2A_OPER_MSI_L1C_TL_SGS__20161201T104644_20161201T141912_A007541_T32TLQ_N02_04_01

8/11/2016: S2A_OPER_MSI_L1C_TL_SGS__20161108T103641_20161108T154744_A007212_T32TMQ_N02_04_01

Sentinel-1:

28/11/2016: S1A_IW_GRDH_1SDV_20161128T053526_20161128T053551_014138_016D3F_7094

22/11/2016: S1B_IW_GRDH_1SDV_20161122T053445_20161122T053514_003067_005376_AD1

Cosmo-Skymed data portal (E-Geos http://www.e-geos.it/)

Image ID 627100 acquired on 25/11/2016 05:11 UTC COSMO-SkyMed© ASI [2016] http://catalog.e-geos.it/#product:productIds=627100 link retrieved 30-03-2018

5-m LIDAR DTM Regione Piemonte is available at:

http://www.geoportale.piemonte.it/geonetworkrp/srv/ita/metadata.show?id=2552&currTab=rndt link retrieved 16-02-2018

Acknowledgments.

The authors gratefully acknowledge Italian Space Agency (ASI) and E-GEOS for the permission of free use of Cosmo-Skymed quick-look data. ARPA and Regione Piemonte for the meteorological and hydrological data of 2016 flood event.

Reference

Ahamed, A., Bolten, J., Doyle, C. and Fayne, J.: Near Real-Time Flood Monitoring and Impact Assessment Systems, In Remote Sensing of Hydrological Extremes (pp. 105-118) Springer International Publishing, doi: 10.1007/978-3-319-43744-6_6, 2017.

Amadio, M., Mysiak, J., Carrera, L. and Koks, E.: Improving flood damage assessment models in Italy, Nat. Hazards, 82(3), 2075-2088, doi: 10.1007/s11069-016-2286-0, 2016.

ARPA Piemonte: Evento alluvionale 21-26 novembre 2016 – rapporto preliminare (Italian), 21-25 November flood event preliminary report, Available at http://www.arpa.piemonte.gov.it/pubblicazioni-2/relazioni-tecniche/analisi-eventi/eventi-2016/rapporto-preliminare-novembre-2016-def.pdf/at_download/file (accessed 1-12-2017), 2016.

Arrighi, C., Brugioni, M., Castelli, F., Franceschini, S. and Mazzanti, B.: Urban micro-scale flood risk estimation with parsimonious hydraulic modelling and census data, Nat. Hazard Earth Sys., 13(5), 13, 1375-1391, https://doi.org/10.5194/nhess-13-1375-2013, 2013.

Barredo, J.I.: Major flood disasters in Europe: 1950–2005, Nat. Hazards, 42(1),125-148, doi: https://doi.org/10.1007/s11069-006-9065-2, 2007.

Bates, P.D. and De Roo, A.P.J: A simple raster-based model for flood inundation simulation, Journal of Hydrology, (236), 54–77 doi: https://doi.org/10.1016/S0022-1694(00)00278-X, 2000.

Bignami, D.F., Rulli, M.C. and Rosso, R.: Testing the use of reimbursement data to obtain damage curves in urbanised areas: the case of the Piedmont flood on October 2000, Journal of Flood Risk Management., doi: https://doi.org/10.1111/jfr3.12292, 2017.

Boccardo, P., Chiabrando, F., Dutto, F., Tonolo, F.G. and Lingua, A.: UAV deployment exercise for mapping purposes: Evaluation of emergency response applications. Sensors, 15(7), pp.15717-15737., doi:10.3390/s150715717, 2015

Boni, G., Ferraris, L., Pulvirenti, L., Squicciarino, G., Pierdicca, N., Candela, L., Pisani, A.R., Zoffoli, S., Onori, R., Proietti, C. and Pagliara, P.: A prototype system for flood monitoring based on flood forecast combined with COSMO-SkyMed and Sentinel-1 data, IEEE Journal of Selected Topics in Applied Earth Observations and Remote Sensing, 9(6), pp.2794-2805, doi: https://doi.org/10.1109/JSTARS.2016.2514402, 2016.

Brakenridge, R. and Anderson, E.; MODIS-based flood detection, mapping and measurement: the potential for operational hydrological applications, Transboundary floods: reducing risks through flood management, 1-12, doi: https://doi.org/10.1007/1-4020-4902-1_1, 2006.

Brivio, P.A., Colombo, R., Maggi, M. and Tomasoni, R.: Integration of remote sensing data and GIS for accurate mapping of flooded areas, International Journal of Remote Sensing, 23(3), 429-441, doi: https://doi.org/10.1080/01431160010014729, 2002.

Buzzi, A., Tartaglione, N. and Malguzzi, P.: Numerical simulations of the 1994 Piedmont flood: Role of orography and moist processes, Monthly Weather Review, 126(9), pp.2369-2383. doi: https://doi.org/10.1175/1520-0493(1998)126<2369:NSOTPF>2.0.CO;2, 1998.

Carraro, F., Collo, G., Forno, M.G., Giardino, M., Maraga, F., Perotto, A., Tropeano, D.: L'evoluzione del reticolato idrografico del Piemonte centrale in relazione alla mobilità quaternaria (Italian)- The evolution of the hidrographic network in the central Piedmont related to the Quaternary mobility- , In: Polino, R., Sacchi, R. (Eds.), Rapporti Alpi-Appennino Accad. Naz. Scienze, (14), 445–461, 1995

Cassardo, C., Cremonini, R., Gandini, D., Paesano, G., Pelosini, R. and Qian, M.W.: Analysis of the severe flood of 13t-16th October 2000 in Piedmont (Italy), Cuadernos de Investigación Geográfica, 27, pp.147-162., DOI: http://dx.doi.org/10.18172/cig.1120, 2013.

Clement, M.A., Kilsby, C.G. and Moore, P.: Multi-Temporal SAR Flood Mapping using Change Detection, Journal of Flood Risk Management, doi: https://doi.org/10.1111/jfr3.12303, 2017.

Copernicus Emergency Management Service (© 2016 European Union), EMSR192 - Floods in Northern Italy, available at http://emergency.copernicus.eu/mapping/list-of-components/EMSR192, (accessed 01/12/17) 2016.

Copernicus Emergency Management Service (© 2016 European Union), [EMSR192] Moncalieri: Grading Map available at http://emergency.copernicus.eu/mapping/list-of-components/EMSR192/ALL/EMSR192_18MONCALIERI (accessed 01/12/17), 2016

Costabile, P., Macchione, F., Natale, L. and Petaccia, G.: Flood mapping using LIDAR DEM. Limitations of the 1-D modeling highlighted by the 2-D approach, Nat. Hazards, 77(1), 181-204, doi: https://doi.org/10.1007/s11069-015-1606-0, 2015.

De Moel, H., Van Alphen, J., and Aerts, J. C. J. H.: Flood maps in Europe – methods, availability and use, Nat. Hazards Earth Syst. Sci., 9, 289-301, https://doi.org/10.5194/nhess-9-289-2009, 2009.

De Zan, F. and Monti-Guarnieri, A., 2006. TOPSAR: Terrain observation by progressive scans, IEEE Transactions on Geoscience and Remote Sensing, 44(9), pp.2352-2360.

Farfaglia, S., Lollino, G., Iaquinta, M., Sale, I., Catella, P., Martino, M. and Chiesa, S.: The use of UAV to monitor and manage the territory: perspectives from the SMAT project, In Engineering Geology for Society and Territory-Volume 5 (pp. 691-695). Springer, Cham, https://doi.org/10.1007/978-3-319-09048-1_134, 2015

Fayne, J., Bolten, J., Lakshmi, V. and Ahamed, A.: Optical and Physical Methods for Mapping Flooding with Satellite Imagery, In Remote Sensing of Hydrological Extremes (pp. 83-103). Springer International Publishing. doi: https://doi.org/10.1007/978-3-319-43744-6_6, 2017.

Feng, Q., Liu, J. and Gong, J.: Urban flood mapping based on unmanned aerial vehicle remote sensing and random forest classifier—A case of Yuyao, China, Water, 7(4), 1437-1455, doi: https://doi.org/10.3390/w7041437, 2015.

Fiorucci, F., Giordan, D., Santangelo, M., Dutto, F., Rossi, M., and Guzzetti, F.: Criteria for the optimal selection of remote sensing images to map event landslides, Nat. Hazards Earth Syst. Sci. Discuss., https://doi.org/10.5194/nhess-2017-111, in review, 2017.

Fohringer, J., Dransch, D., Kreibich, H. and Schröter, K.: Social media as an information source for rapid flood inundation mapping, Nat. Hazard Earth Sys, 15(12), 2725-2738, doi: https://doi.org/10.5194/nhess-15-2725-2015, 2015.

Gao, B.C.: NDWI—A normalized difference water index for remote sensing of vegetation liquid water from space, Remote sensing of environment, 58(3), 257-266, doi: https://doi.org/10.1016/S0034-4257(96)00067-3, 1996.

Gianinetto, M., Villa, P. and Lechi, G.: Postflood damage evaluation using Landsat TM and ETM+ data integrated with DEM, IEEE Transactions on Geoscience and Remote Sensing, 44(1), 236-243, doi: https://doi.org/10.1109/TGRS.2005.859952, 2006.

Giordan, D., Manconi, A., Facello, A., Baldo, M., Allasia, P. and Dutto, F.: Brief Communication: The use of an unmanned aerial vehicle in a rockfall emergency scenario, Nat. Hazards Earth Syst. Sci., 15(1), pp.163-169, doi: https://doi.org/10.5194/nhess-15-163-2015, 2015.

Giordan D., Manconi A., Remondino F. and Nex F.: Use of unmanned aerial vehicles in monitoring application and management of natural hazards, Geomatics, Natural Hazards and Risk, 8:1, 1-4, DOI: https://doi.org/10.1080/19475705.2017.1315619, 2017.

Giustarini, L., Hostache, R., Matgen, P., Schumann, G. J. P., Bates, P. D. and Mason, D. C.: A change detection approach to flood mapping in urban areas using TerraSAR-X, IEEE transactions on Geoscience and Remote Sensing, 51(4), 2417-2430. doi: 0.1109/TGRS.2012.2210901, 2013.

Griesbaum, L., Marx, S. and Höfle, B.: Direct local building inundation depth determination in 3-D point clouds generated from user-generated flood images. Natural Hazards and Earth System Sciences, 17(7), p.1191, 2017.

Hung, K.C., Kalantari, M. and Rajabifard, A.: Methods for assessing the credibility of volunteered geographic information in flood response: A case study in Brisbane, Australia, Applied Geography, 68, 37-47, doi: https://doi.org/10.1016/j.apgeog.2016.01.005, 2016.

Ireland, G., Volpi, M. and Petropoulos, G.P.: Examining the capability of supervised machine learning classifiers in extracting flooded areas from Landsat TM imagery: A case study from a Mediterranean flood, Remote Sensing, 7(3), 3372-3399, doi: https://doi.org/10.3390/rs70303372, 2015.

Justice, C.O., Vermote, E., Townshend, J.R., Defries, R., Roy, D.P., Hall, D.K., Salomonson, V.V., Privette, J.L., Riggs, G., Strahler, A. and Lucht, W.: The Moderate Resolution Imaging Spectroradiometer (MODIS): Land remote sensing for global change research, IEEE Transactions on Geoscience and Remote Sensing, 36(4), 1228-1249, 1998.

Kreibich, H., Piroth, K., Seifert, I., Maiwald, H., Kunert, U., Schwarz, J., Merz, B. and Thieken, A.H.: Is flow velocity a significant parameter in flood damage modelling?, Nat. Hazards Earth Syst. Sci., 9, 1679-1692, https://doi.org/10.5194/nhess-9-1679-2009, 2009.

Luino, F., Cirio, C.G., Biddoccu, M., Agangi, A., Giulietto, W., Godone, F. and Nigrelli, G.: Application of a model to the evaluation of flood damage, Geoinformatica, 13(3), 339-353, doi: 10.1007/s10707-008-0070-3, 2009.

Luino, F.: The flood and landslide event of November 4–6 1994 in Piedmont Region (Northwestern Italy): Causes and related effects in Tanaro Valley, Physics and Chemistry of the Earth, Part A: Solid Earth and Geodesy, 24(2), 123-129, doi: https://doi.org/10.1016/S1464-1895(99)00007-1, 1999.

Mason D.C., Giustarini L., Garcia-Pintado J., Cloke H.L.: Detection of flooded urban areas in high resolution Synthetic Aperture Radar images using double scattering, International Journal of Applied Earth Observation and Geoinformation, Volume 28, Pages 150-159, ISSN 0303-2434, http://dx.doi.org/10.1016/j.jag.2013.12.002, 2014.

Meesuk, V., Vojinovic, Z., Mynett, A.E. and Abdullah, A.F.: Urban flood modelling combining top-view LiDAR data with ground-view SfM observations, Advances in Water Resources, 75, 105-117, doi: https://doi.org/10.1016/j.advwatres.2014.11.008, 2015.

Merz, B., Kreibich, H., Schwarze, R., and Thieken, A.: Review article "Assessment of economic flood damage", Nat. Hazards Earth Syst. Sci., 10, 1697-1724, https://doi.org/10.5194/nhess-10-1697-2010, 2010.Nigro, J., Slayback, D., Policelli, F. and Brakenridge, G.R.: NASA/DFO MODIS near real-time (NRT) global flood mapping product evaluation of flood and permanent water detection. Evaluation, Greenbelt, MD, 2014.

Paprotny, D., Morales-Nápoles, O., and Jonkman, S. N.: Efficient pan-European river flood hazard modelling through a combination of statistical and physical models, Nat. Hazards Earth Syst. Sci., 17, 1267-1283, https://doi.org/10.5194/nhess-17-1267-2017, 2017.

Perks, M. T., Russell, A. J., and Large, A. R. G.: Technical Note: Advances in flash flood monitoring using unmanned aerial vehicles (UAVs), Hydrol. Earth Syst. Sci., 20, 4005-4015, https://doi.org/10.5194/hess-20-4005-2016, 2016.

Pierdicca, N., Pulvirenti, L. and Chini, M.: Flood Mapping in Vegetated and Urban Areas and Other Challenges: Models and Methods. In Flood Monitoring through Remote Sensing (pp. 135-179). Springer, Cham., https://doi.org/10.1007/978-3-319-63959-8_7, 2018

Pinto, J.G., Ulbrich, S., Parodi, A., Rudari, R., Boni, G. and Ulbrich, U.: Identification and ranking of extraordinary rainfall events over Northwest Italy: The role of Atlantic moisture, Journal of Geophysical Research: Atmospheres, 118(5), 2085-2097, doi: https://doi.org/10.1002/jgrd.50179, 2013.

Pulvirenti, L., Chini, M., Pierdicca, N., Guerriero, L. and Ferrazzoli, P.: Flood monitoring using multi-temporal COSMO-SkyMed data: Image segmentation and signature interpretation, Remote Sensing of Environment, 115(4),990-1002, doi: https://doi.org/10.1016/j.rse.2010.12.002, 2011.

Rahman, M.S. and Di, L.: The state of the art of spaceborne remote sensing in flood management, Natural Hazards, 85(2), 1223-1248., doi: https://doi.org/10.1007/s11069-016-2601-9, 2017.

Refice, A., Capolongo, D., Pasquariello, G., D'Addabbo, A., Bovenga, F., Nutricato, R., Lovergine, F.P. and Pietranera, L.: SAR and InSAR for flood monitoring: Examples with COSMO-SkyMed data, IEEE Journal of Selected Topics in Applied Earth Observations and Remote Sensing, 7(7), 2711-2722, doi: https://doi.org/10.1109/JSTARS.2014.2305165, 2014.

Regione Piemonte: Gli eventi alluvionali del settembre-ottobre 1993 in Piemonte (Italian), http://www.arpa.piemonte.gov.it/approfondimenti/temi-ambientali/geologia-e-dissesto/pubblicazioni/immagini-e-files/ev93, (accessed 01/12/17), 1996.

Rosser, J.F., Leibovici, D.G. and Jackson, M.J.: Rapid flood inundation mapping using social media, remote sensing and topographic data, Natural Hazards, 87(1), 103-120, doi: https://doi.org/10.1007/s11069-017-2755-0, 2017.

Segura-Beltrán, F., Sanchis-Ibor, C., Morales-Hernández, M., González-Sanchis, M., Bussi, G. and Ortiz, E.: Using post-flood surveys and geomorphologic mapping to evaluate hydrological and hydraulic models: The flash flood of the Girona River (Spain) in 2007, Journal of Hydrology, 541, pp.310-329. https://doi.org/10.1016/j.jhydrol.2016.04.039, 2016.

Schnebele, E. and Cervone, G.: Improving remote sensing flood assessment using volunteered geographical data, Nat. Hazards Earth Syst. Sci., 13, 669-677, https://doi.org/10.5194/nhess-13-669-2013, 2013.

Shrestha, R., Di, L., Eugene, G.Y., Kang, L., SHAO, Y.Z. and BAI, Y.Q.: Regression model to estimate flood impact on corn yield using MODIS NDVI and USDA cropland data layer, Journal of Integrative Agriculture, 16(2), 398-407, doi: https://doi.org/10.1016/S2095-3119(16)61502-2, 2017.

Smith, M. W., J. L. Carrivick, J. Hooke, and Kirkby M. J.: Reconstructing flash flood magnitudes using 'Structure-from-Motion': A rapid assessment tool, Journal of Hydrology 519, pp 1914-1927, doi: https://doi.org/10.1016/j.jhydrol.2014.09.078, 2014.

Schumann, G.J.P. and Moller, D.K.: Microwave remote sensing of flood inundation. Physics and Chemistry of the Earth, Parts A/B/C, 83, pp.84-95., doi: https://doi.org/10.1016/j.pce.2015.05.002, 2015

Snavely, N., Seitz, S.M. and Szeliski, R.: Modelling the world from internet photo collections, International Journal of Computer Vision, 80(2), 189-210, doi: https://doi.org/10.1007/s11263-007-0107-3, 2008.

Tapia-Silva, F.O., Itzerott, S., Foerster, S., Kuhlmann, B. and Kreibich, H.: Estimation of flood losses to agricultural crops using remote sensing, Physics and Chemistry of the Earth, Parts A/B/C, 36(7), 253-265, doi: https://doi doi.org/10.1016/j.pce.2011.03.005, 2011.

Torres, R., Snoeij, P., Geudtner, D., Bibby, D., Davidson, M., Attema, E., Potin, P., Rommen, B., Floury, N., Brown, M. and Traver, I.N.: GMES Sentinel-1 mission, Remote Sensing of Environment, 120, pp.9-24, doi: https://doi.org/10.1016/j.rse.2011.05.028, 2012.

Vermote E. - NASA GSFC and MODAPS SIPS – NASA: MYD09 MODIS/Aqua L2 Surface Reflectance, 5-Min Swath 250m, 500m, and 1km. NASA LP DAAC, doi: http://doi.org/10.5067/MODIS/MYD09.006, 2015

Yan, K., Di Baldassarre, G., Solomatine, D.P. and Schumann, G.J.P.: A review of low-cost space-borne data for flood modelling: topography, flood extent and water level, Hydrological Processes, 29(15), 3368-3387, doi: https://doi.org/10.1002/hyp.10449, 2015.

Wang, Y., Colby, J.D. and Mulcahy, K.A.: An efficient method for mapping flood extent in a coastal floodplain using Landsat TM and DEM data, International Journal of Remote Sensing, 23(18), 3681-3696, doi: https://doi.org/10.1080/01431160110114484, 2012.

Westoby, M. J., J. Brasington, N. F. Glasser, M. J. Hambrey, and Reynolds J.M.: 'Structure-from-Motion' photogrammetry: A low-cost, effective tool for geoscience applications, Geomorphology 179, 300-314, doi: https://doi.org/j.geomorph.2012.08.02, 2012.

Xu, H.: Modification of normalised difference water index (NDWI) to enhance open water features in remotely sensed imagery, International journal of remote sensing, 27(14), 3025-3033, doi: https://doi.org/10.1080/01431160600589179, 2006.

Zhang, D. and Zhou, G.: Estimation of Soil Moisture from Optical and Thermal Remote Sensing: A Review, Sensors, 16(8), p.1308, doi: https://doi.org/1016/j.pce.2011.03.005, 2016.

Table 1. Resume of the datasets used to map and characterize flooded area in this study

Type	Sensor used	Spatial resolution (m)	Covered area by a single scene (km^2)	Min. Revisit time (Day)
		1 – Satellite Data		
SAR –X band	Cosmo-SkyMed	60	> 1'000	4
SAR- C band	Sentinel-1A/B	5 (ground range) x 20 (azimuth)	> 10'000	6
Multi-spectral	MODIS-Aqua	500	> 100'0000	Daily
Multi-spectral	Sentinel-2	10 / 20	> 10'000	10 (5)
		2- Aerial data		
Very High res. visible band	Tecnam P92-JS	0.01	100 km^2	On-demand
Ultra-High resolution visible band	RPASs CarbonCore 950 octocopter	0.02 / 0.03	< 10 km^2	On-demand
DTM LIDAR	Airborne	5	Piemonte region	Archive data
		3- Ground-Based		
Photo / video from car platform	GO-PRO HERO 3+	0.02 / 0.03	Local /urban	On demand

Table 2. Resume of satellite data in relation with flood stage

Satellite	Spatial Resolution	Acquisition time		
		Pre-flood	Co-flood	Post-flood
Cosmo-SkyMed	Medium		05:05 UTC – 25/11/2016	
Sentinel-1 A/B	Medium	05:35 UTC – 22/11/2016		05:35 UTC – 28/11/2016
MODIS Aqua	Medium-Low	12:30 UTC - 12/11/2016	12:30 UTC - 26/11/2016	
Sentinel-2	Medium-High	15:19 UTC - 11/11/2016		14:19 UTC – 01/12/2016

815

Table 3. Characteristics of the Sentinel-1 dataset used in this study

Satellite	Sentinel-1 A/B
Sensor Parameter	C-band 5.405 GHz
Orbit	Descending
Pre-flood acquisitions	22/11/2016
Post-flood acquisitions	28/11/2016
Data format	Single Look Complex (SLC)
Azimuth pixel spacing [m]	~13

Range pixel spacing [m]	~2

Table 4. Characteristics of the Aqua MODIS data used in this work.

Band	Bandwidth nm	Band type	Spatial resolution (m)
B1	620 – 670	Red	500
B2	841 – 876	NIR	500
B3	459 – 479	Blue	500
B4	545 – 565	Green	500
B5	1230 – 1250	SWIR	500
B7	2105 – 2155	SWIR	500

820

Table 5. Characteristics of Sentinel-2 data used in this work.

Band	Wavelength nm	Band type	Spatial resolution (m)
B2	490	Blue	10
B3	560	Green	10
B4	665	Red	10
B8	842	NIR	10
B5	705	NIR	20
B6	740	NIR	20
B7	783	NIR	20
B8a	865	NIR	20
B11	1610	SWIR	20
B12	2190	SWIR	20

Table 6. Accuracy in automatic flooded and not flooded area detection

Sector	Area	Sentinel-2		MODIS-Aqua			CSKM	Sentinel-1
	km^2	$MNDWI_{var}$	$NDVI_{var}$	$MNDWI_{var}$	MLC	SA	Recl Ampl	$\Delta\sigma^o$
Not Flooded	259.5	87%	87%	91%	94%	95%	96%	99%
Flooded area								
- Po	47.8	48%	37%	49%	70%	64%	23%	4%
- Oitana	11.6	49%	42%	60%	11%	36%	37%	1%
- Chisola	7.3	21%	51%	30%	24%	23%	12%	1%

- Chisola urban	1.1	4%	24%

825

Table 7. Water height measures obtained from structure-from-motion, GPS survey and simulation with DTM

Measure point coordinates		Water Depth (m)		
UTM X	UTM Y	SfM (+/- 0.05)	GPS	DTM (+/- 0.2)
395132	4983240	1.56	1.60	1.61
395242	4983152	1.45	1.40	1.42
395140	4982644	0.84	0.78	1.01
395142	4981624	0.82	0.81	0.78
395022	4981188	1.28	1.35	1.56
394877	4980993	1.40	1.37	1.34

830

835

840

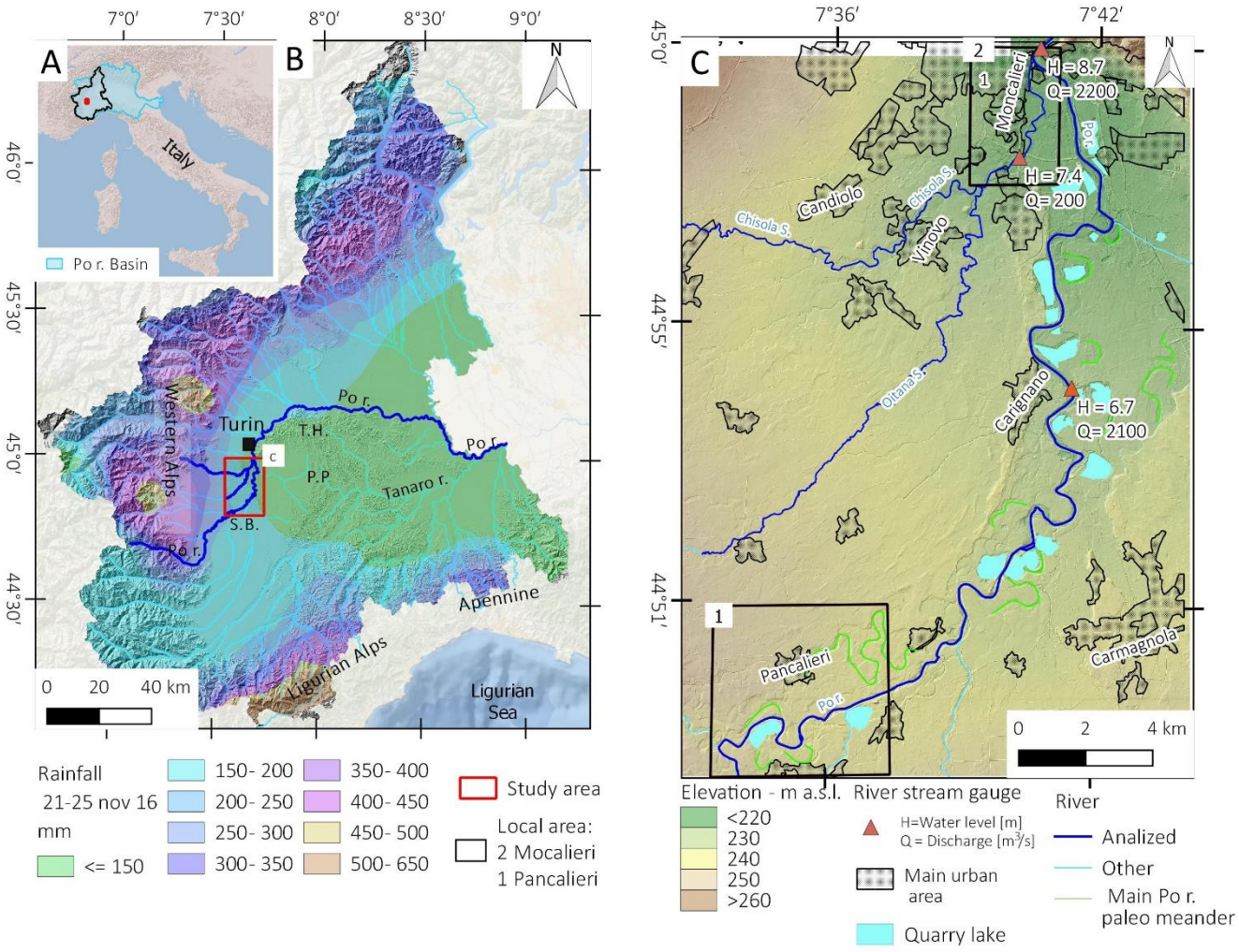

Figure 1: A) Location of Piemonte region in Italy; B) Rainfall in Piemonte region during the 21-25 November flood event (Based on ARPA Piemonte data) and location of study area, S. B. = Savigliano Basin, P. P. = Poirino Plateau, T.H = Turin Hills; C) Detailed view of the study area with discharge in the stream gauge stations and the location of Pancalieri (1) and Moncalieri (2) local areas case history.

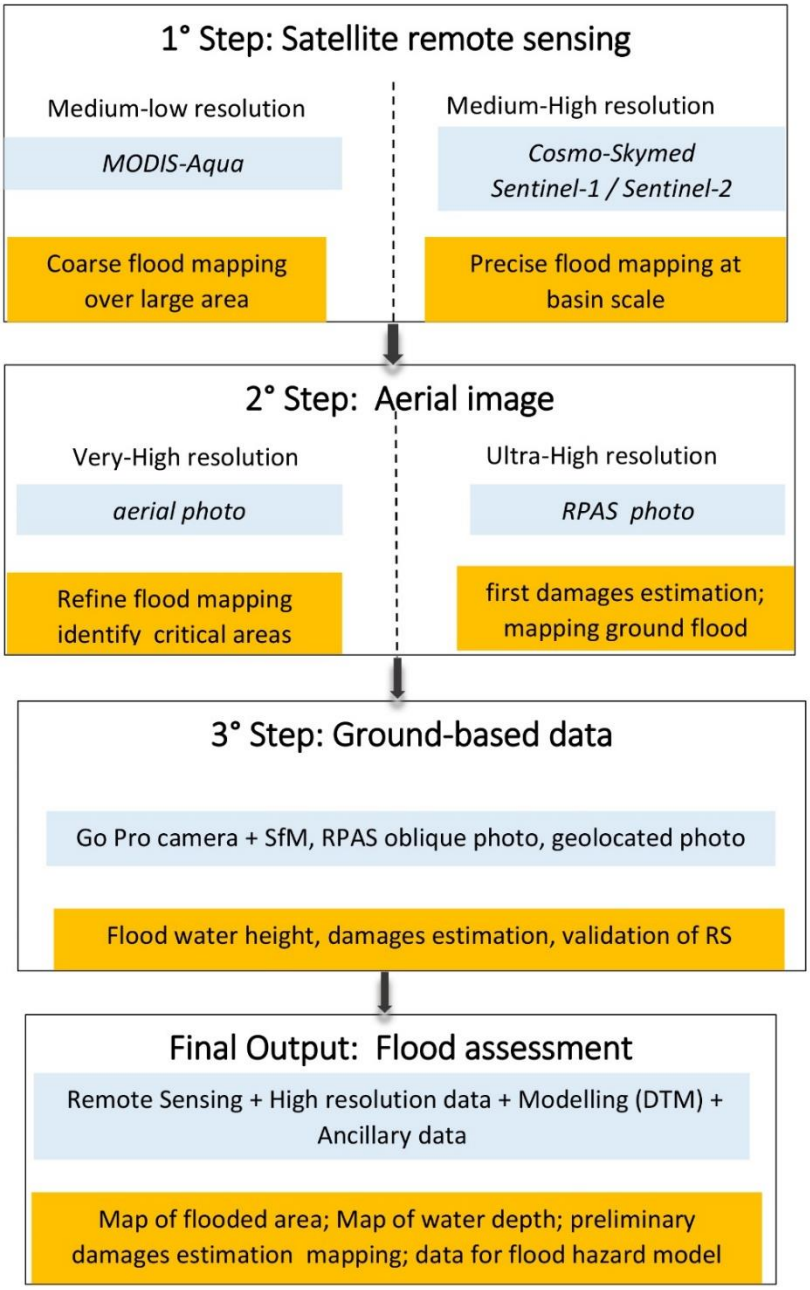

Figure 2: The flowchart illustrating the multiscale flood mapping approaches proposed in this work

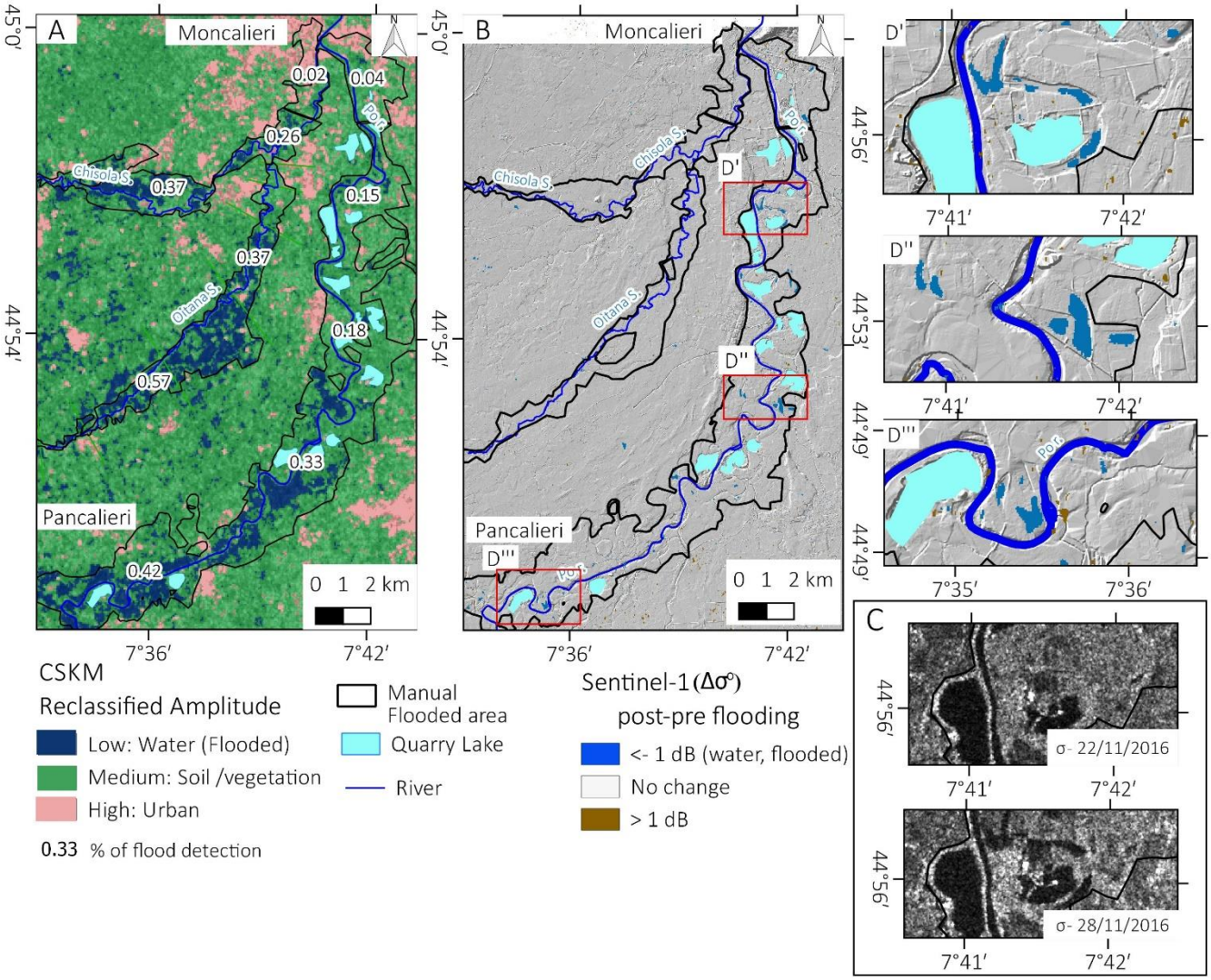

850

Figure 3: A) Reclassified Quicklook Amplitude SAR Image acquired at 05:05 UTC of 25 November 2016 - COSMO-SkyMed© ASI [2016] - B) Sentinel-1 geocoded backscattering coefficient difference (Δσ°); **C) Example of change backscattering between the pre- and the post-flood image is detectable.** D'; D'' D''') **detail of some areas where** Δσ° **still detect water.**

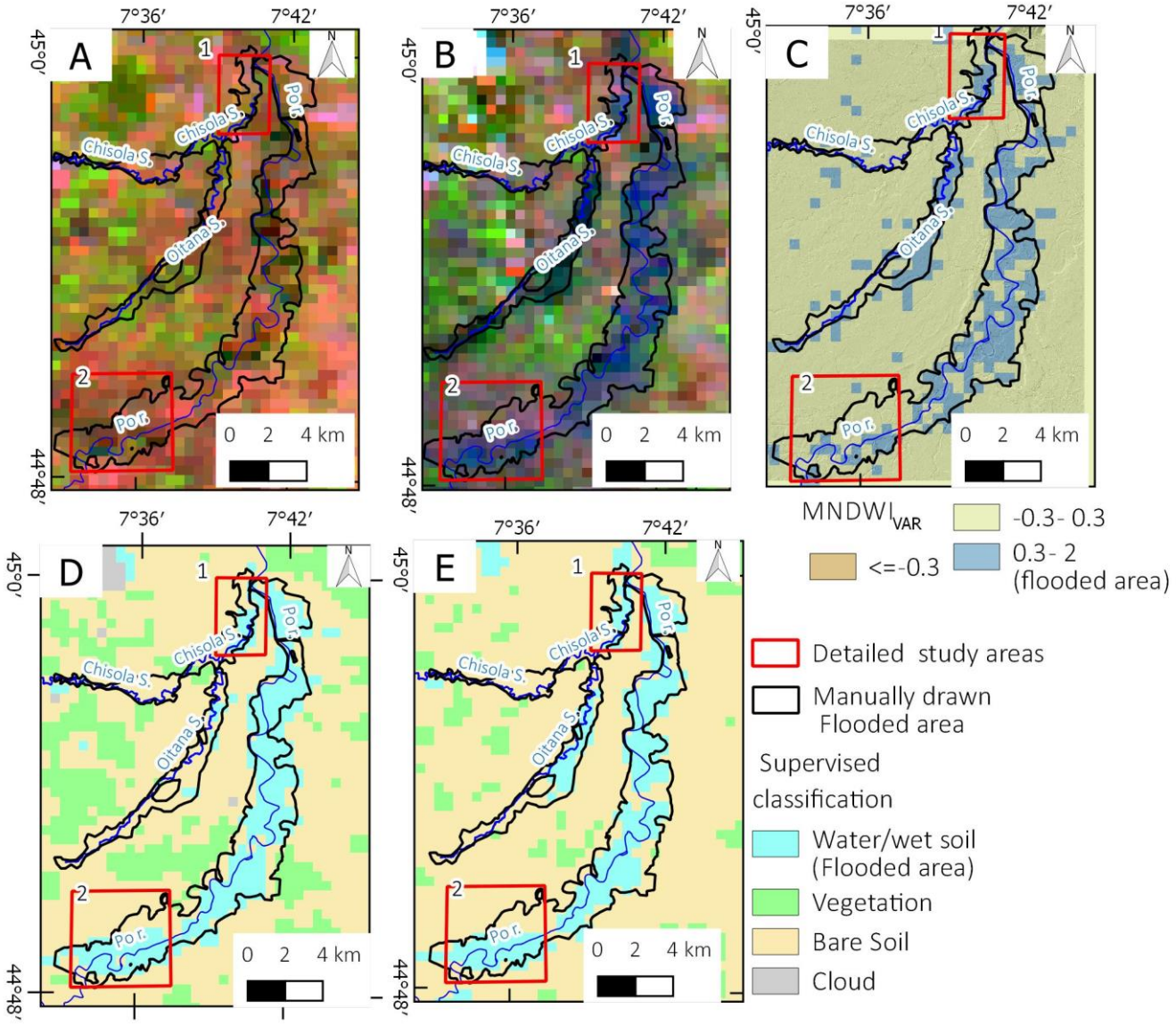

855 **Figure 4: MODIS Aqua satellite image A) False colour band composition 7-2-1 acquired the 12 November 2016.; B) False colour band composition 7-2-1 acquired the 26 November 2016.; C) automatic detection of the flooded area using $MNDWI_{var}$>0.3; automatic detection of the flooded area using supervised classification with maximum likelihood method (D) and with spectral angle method (E). The red box identifies the local case history of Moncaleri (1) and Pancalieri (2)**

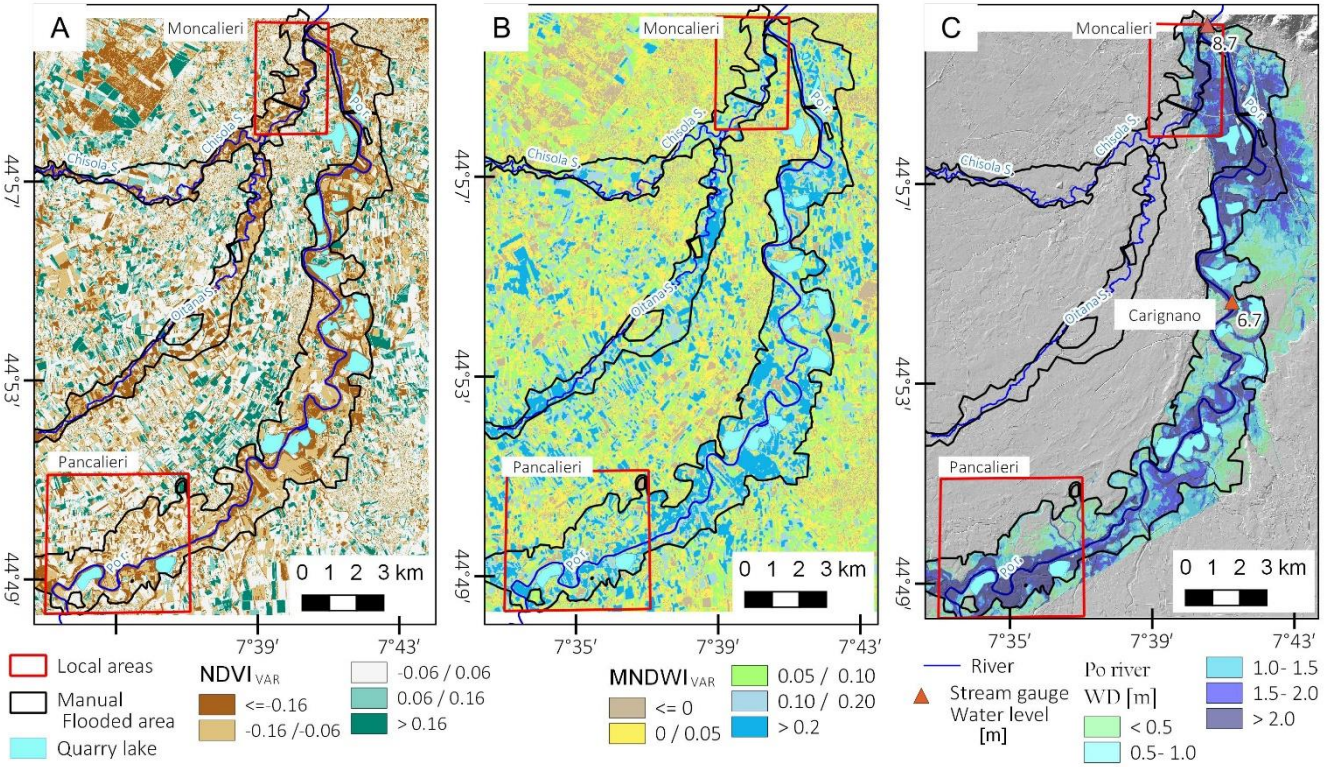

Figure 5: Sentinel-2 analysis and validation: A) NDVI variation 10 m of spatial resolution, B) MNDWI variation 20 m of spatial resolution, C) Simulation of flooded area water depth for Po river based on 5-m DTM and river height level registered in Arpa Piemonte stream gauge.

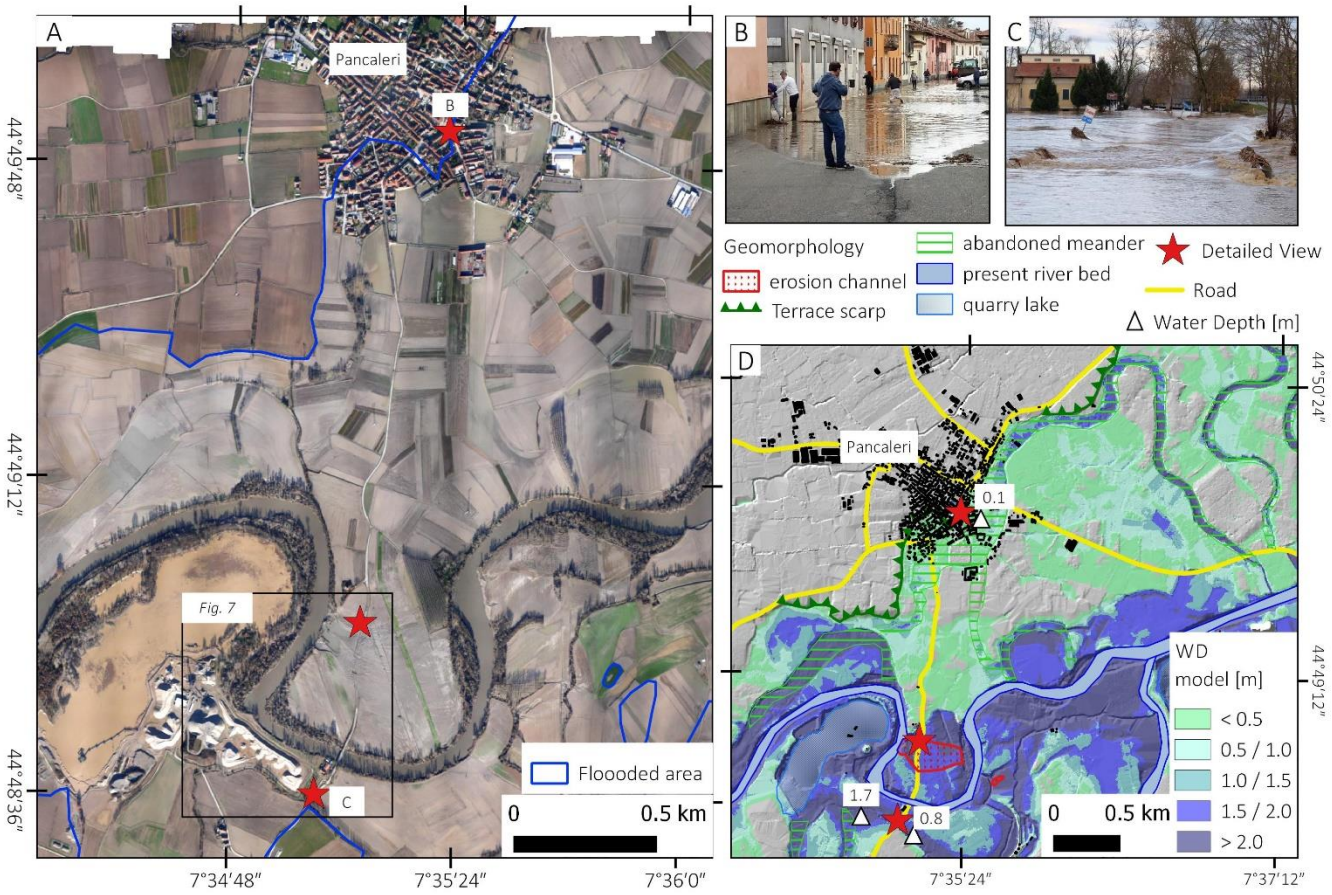

Figure 6: A) Aerial photo at 10 cm of resolution taken the 28 November 2016; B and C) photo took from a local newspaper and geolocalized with Google Streetview; D) Geomorphological elements and model of estimated water depth (m).

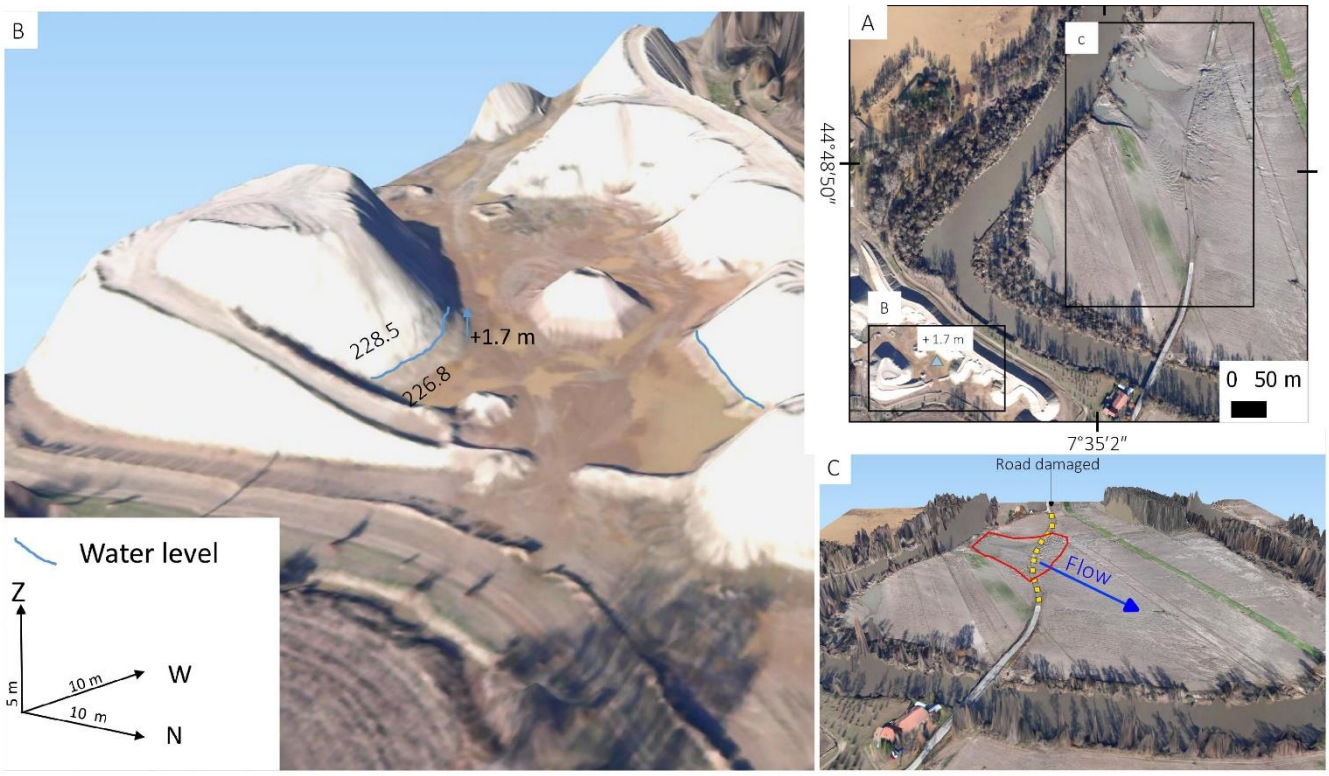

Figure 7: The SfM 3-D model obtained from very high-resolution aerial photo, near Po River at the south of Pancalieri (A) allowed: B) Measuring the approximate water depth on a sand deposits of a quarry (A); C) Mapping the effect of meander cut a: an erosion channel and the destruction along a stretch of road.

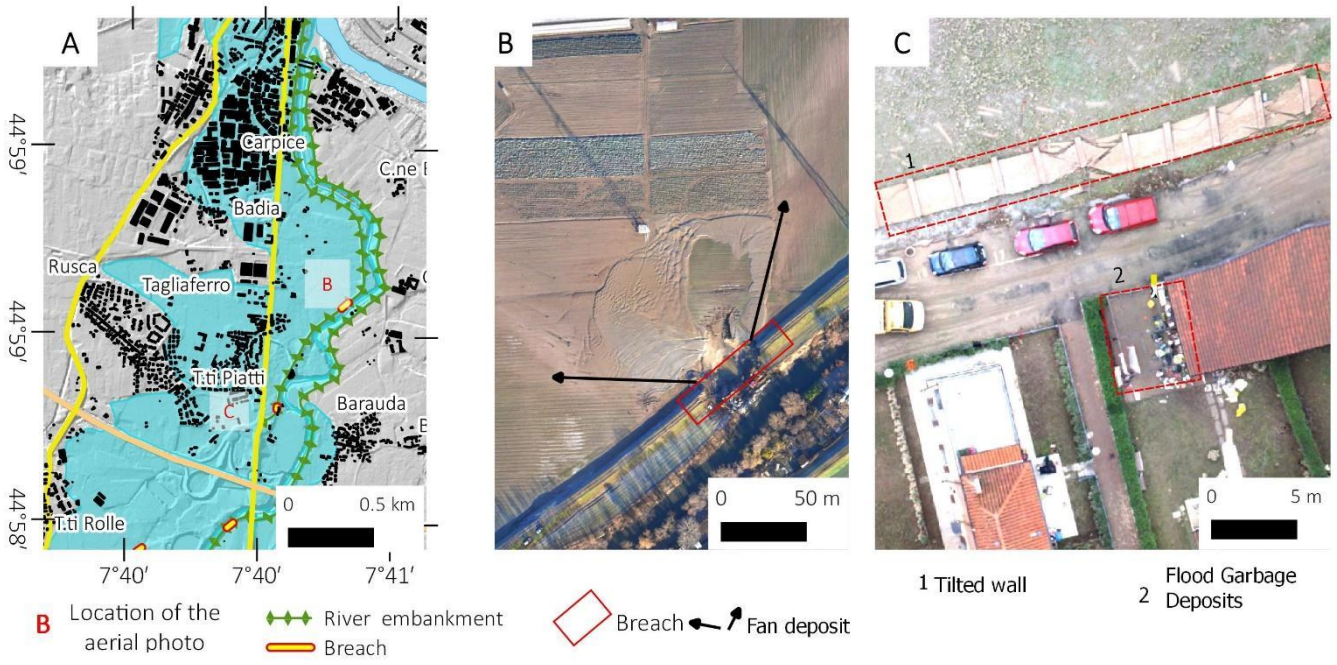

Figure 8: A) map of flooded Chisola flooded area in Moncalieri municipality with location of detailed photo; B) Aerial photo at 0.1 m of resolution showing the breach of river embankment and the 'alluvial fan' created by water flow showed with a 3-d view in figure 9; C) RPASs photo at 0.02 m of spatial resolution showing a collapsed wall in the Tetti Piatti area and a deposit of damaged good from the nearby house.

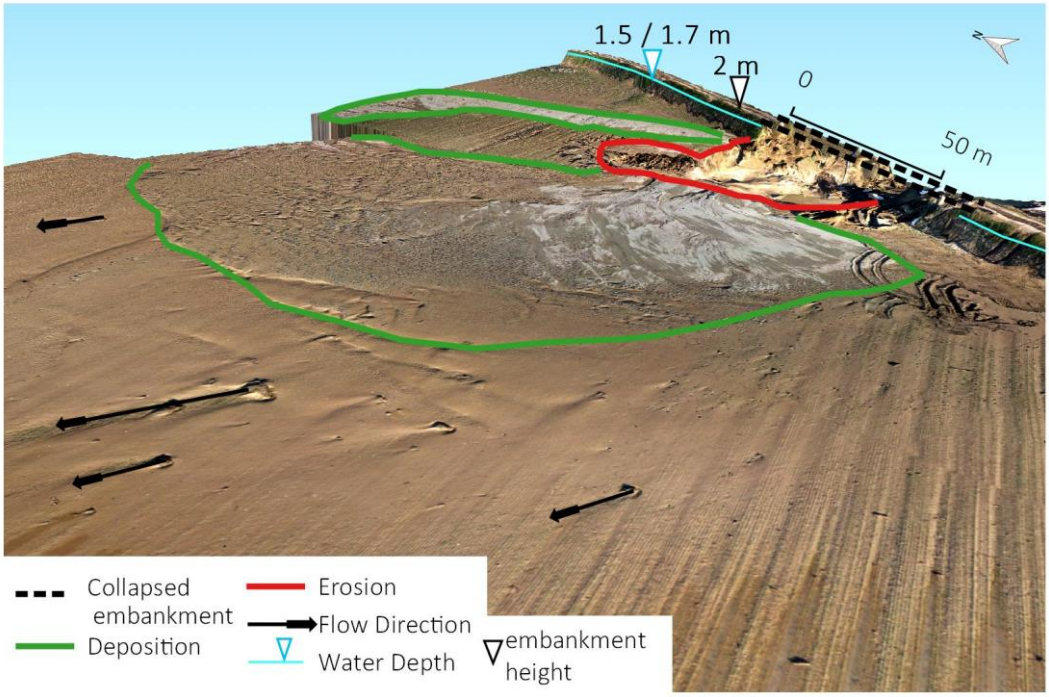

880

Figure 9: 3-D Model derived from the RPASs aerial photo and SfM elaborations photo overlap. The model shows the river embankment rupture (point B in figure 8A), the geomorphological effects in the neighbour areas. It is also possible to estimate water depth from the signs on the embankment.

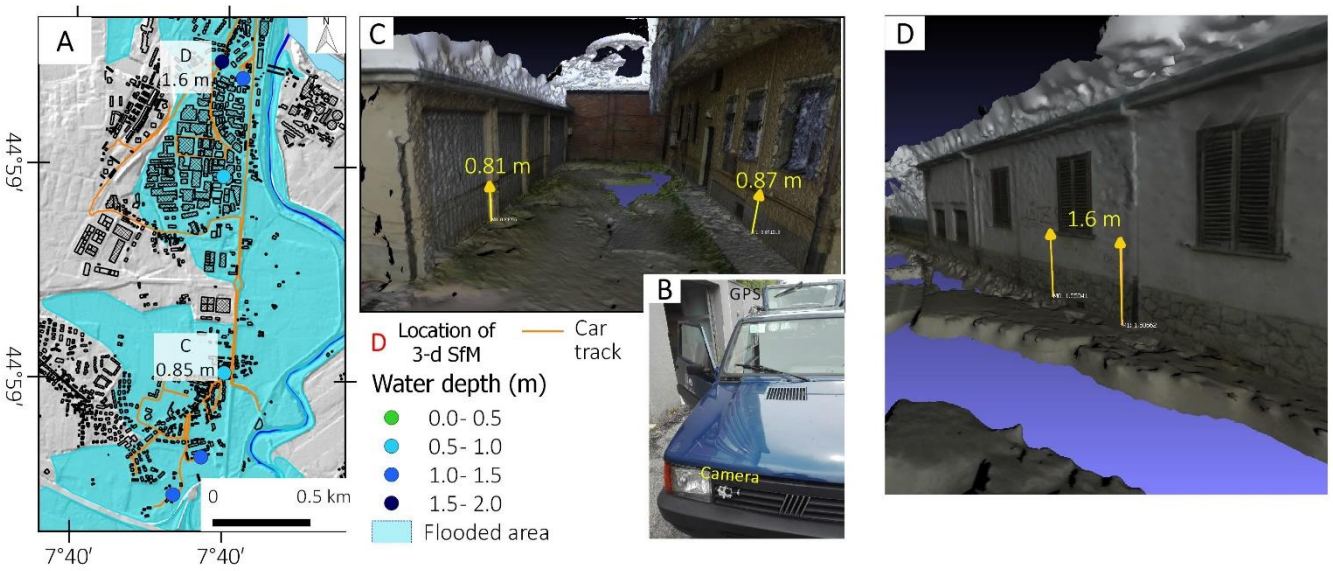

885 **Figure 10: A) Map of the flooded area by Chisola stream in the Moncalieri municipality with measured water height and location of 3-d photo; B) Installation of the GO-PRO HERO 3+ (Black Edition) camera and GPS antenna over the car (the processing system for STANAG 4609 encoding was installed inside the car); C and D) Examples 3-d models made with Structure from Motion in which was possible to measure the water height. .**

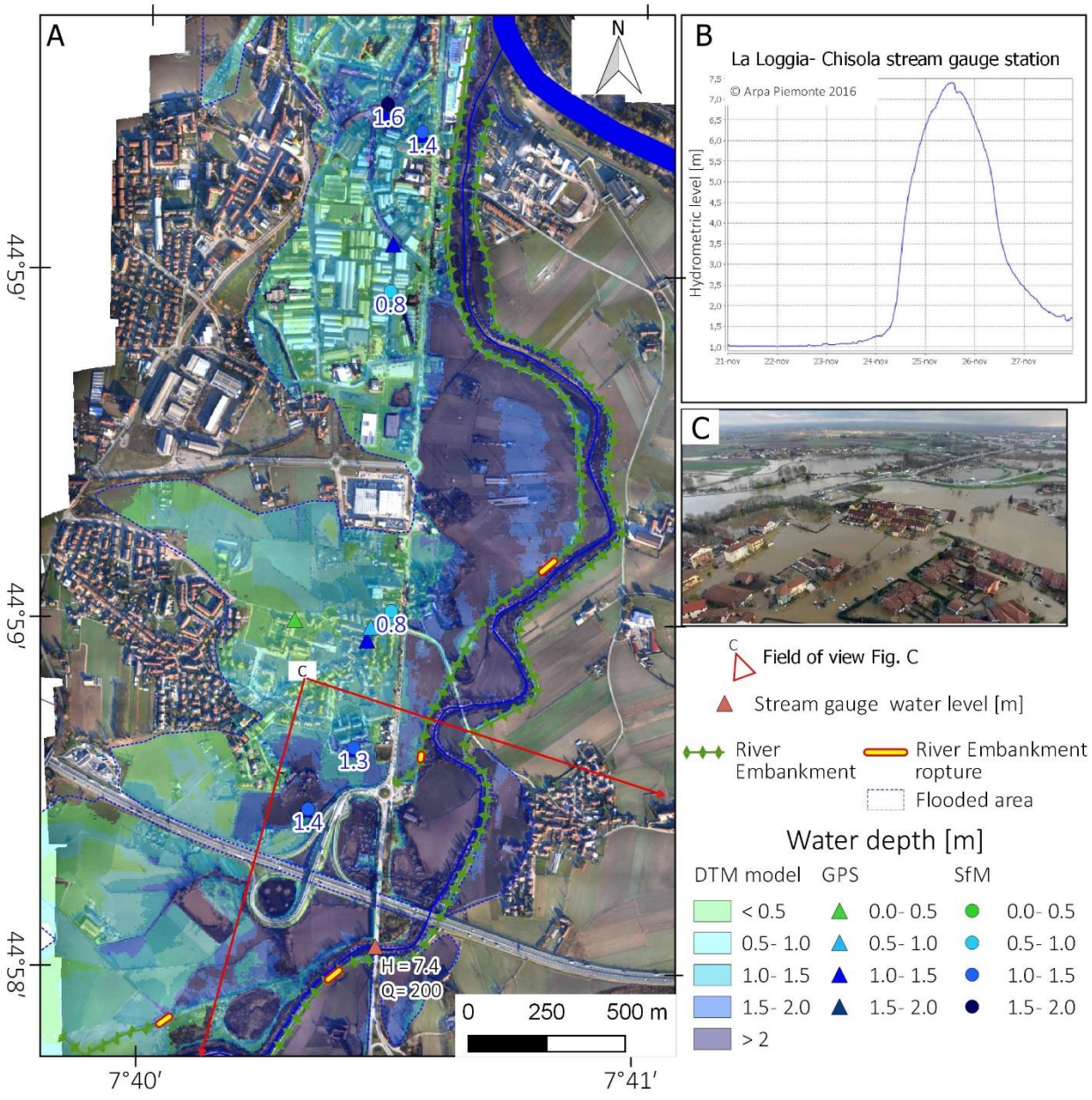

890

Figure 11: A) Water depth levee map based on SfM data and 5-m DTM model; B) Water level reached by Chisola stream in ARPA Piemonte station; C) Geolocated third part photo: 25/11/2016 aerial view of flooded area find on the web (https://vivere-moncalieri.it/2016/11/30/3760/)

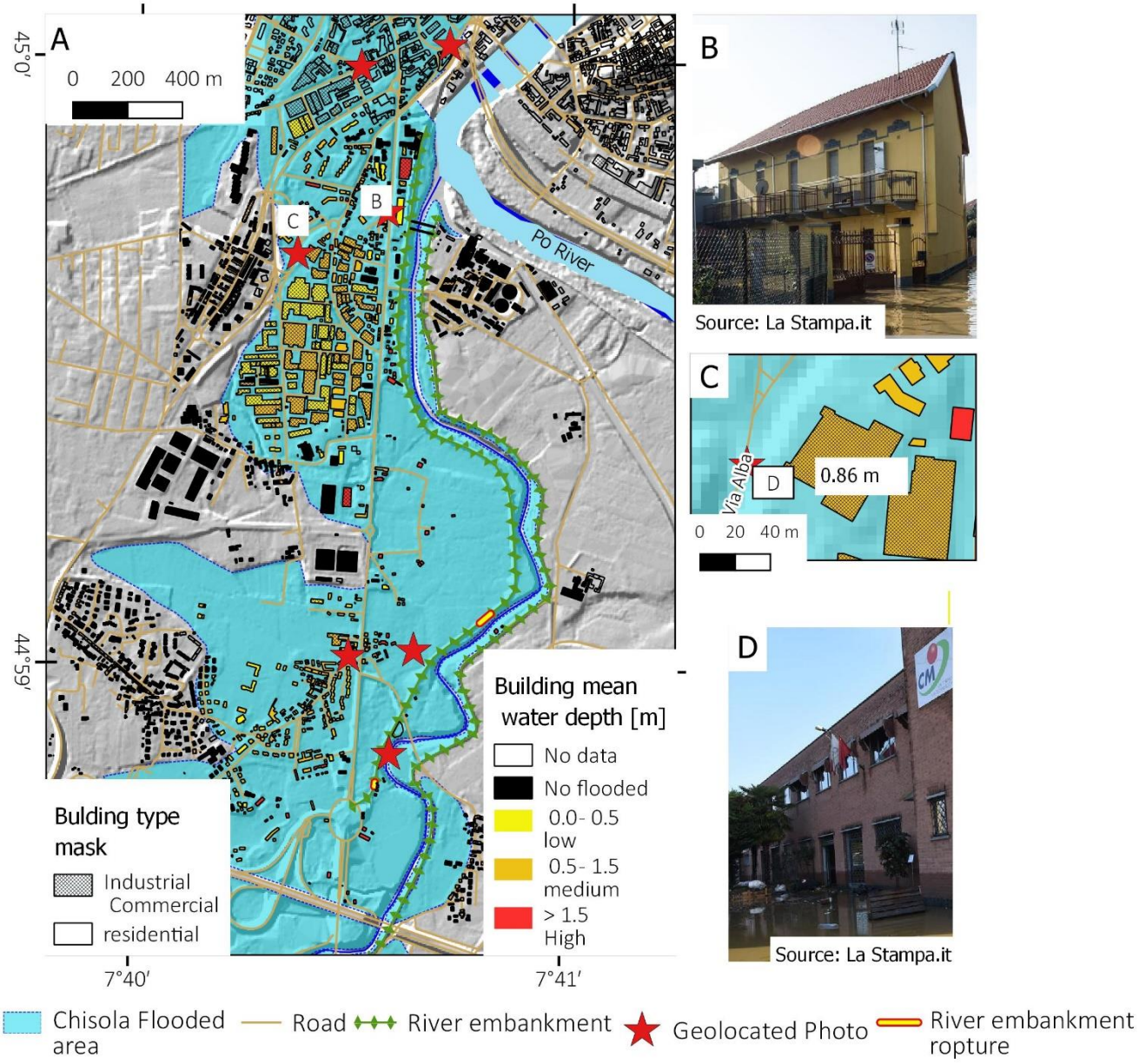

Figure 12: A) Water level height map based on SfM data and 5-m DTM model; C) Zoom on the building of figure D; B and D) Photo where it is possible to observe the water depth from the newspaper "La Stampa" geolocated using Google Street view.

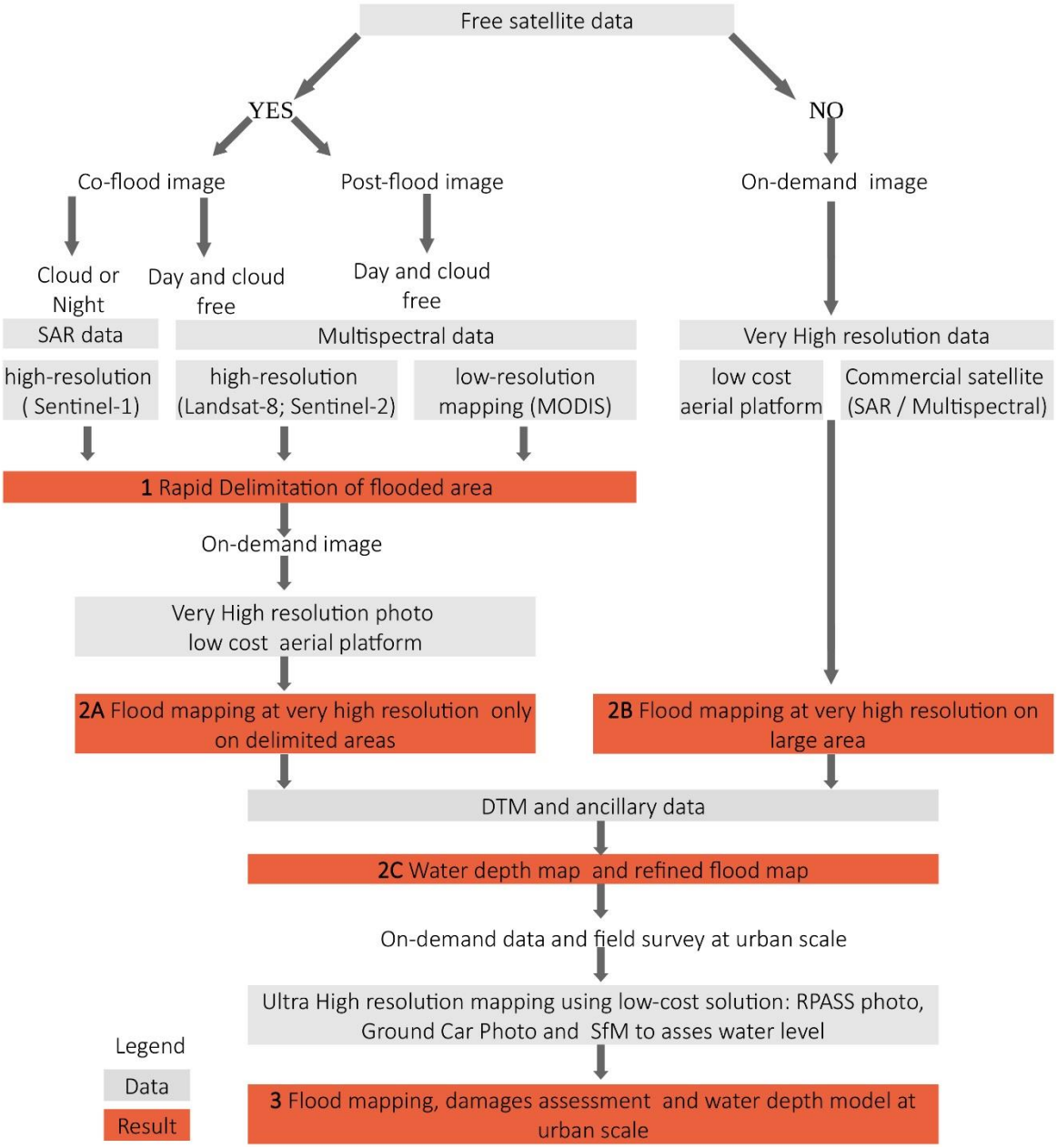

900 **Figure 13: Flowchart of the proposed flood mapping strategy**